

# The underluminous Type Ia Supernova 2005bl and the class of objects similar to SN 1991bg\*

S. Taubenberger<sup>1</sup> †, S. Hachinger<sup>1</sup>, G. Pignata<sup>2,3</sup>, P. A. Mazzali<sup>1,4</sup>, C. Contreras<sup>5</sup>, S. Valenti<sup>6,7</sup>, A. Pastorello<sup>1,8</sup>, N. Elias-Rosa<sup>1,9,10</sup>, O. Bärnbantner<sup>11</sup>, H. Barwig<sup>11</sup>, S. Benetti<sup>9</sup>, M. Dolci<sup>12</sup>, J. Fliri<sup>11</sup>, G. Folatelli<sup>5</sup>, W. L. Freedman<sup>13</sup>, S. Gonzalez<sup>5</sup>, M. Hamuy<sup>2</sup>, W. Krzeminski<sup>5</sup>, N. Morrell<sup>5</sup>, H. Navasardyan<sup>9</sup>, S. E. Persson<sup>13</sup>, M. M. Phillips<sup>5</sup>, C. Ries<sup>11</sup>, M. Roth<sup>5</sup>, N. B. Suntzeff<sup>14</sup>, M. Turatto<sup>9</sup> and W. Hillebrandt<sup>1</sup>

<sup>1</sup>Max-Planck-Institut für Astrophysik, Karl-Schwarzschild-Str. 1, 85741 Garching bei München, Germany

<sup>2</sup>Departamento de Astronomía, Universidad de Chile, Casilla 36-D, Santiago, Chile

<sup>3</sup>Departamento de Astronomía y Astrofísica, Pontificia Universidad Católica de Chile, Casilla 306, Santiago 22, Chile

<sup>4</sup>INAF Osservatorio Astronomico di Trieste, Via Tiepolo 11, 34131 Trieste, Italy

<sup>5</sup>Las Campanas Observatory, Carnegie Observatories, Casilla 601, La Serena, Chile

<sup>6</sup>European Southern Observatory (ESO), Karl-Schwarzschild-Str. 2, 85748 Garching bei München, Germany

<sup>7</sup>Physics Department, University of Ferrara, 44100 Ferrara, Italy

<sup>8</sup>Astrophysics Research Centre, School of Mathematics and Physics, Queen's University Belfast, Belfast BT7 1NN, UK

<sup>9</sup>INAF Osservatorio Astronomico di Padova, Vicolo dell'Osservatorio 5, 35122 Padova, Italy

<sup>10</sup>Universidad de La Laguna, Av. Astrofísico Francisco Sánchez s/n, E-38206 La Laguna, Tenerife, Spain

<sup>11</sup>Universitäts-Sternwarte München, Scheinerstr. 1, 81679 München, Germany

<sup>12</sup>INAF Osservatorio Astronomico di Collurania Teramo, Via Maggini, 64100 Teramo, Italy

<sup>13</sup>Observatories of the Carnegie Institution of Washington, Pasadena, CA, USA

<sup>14</sup>Texas A&M University Physics Department, College Station, TX, USA

Accepted 2007 November 28; received 2007 November 27; in original form 2007 October 11.

## ABSTRACT

Optical observations of the Type Ia supernova (SN Ia) 2005bl in NGC 4070, obtained from  $-6$  to  $+66$  d with respect to the  $B$ -band maximum, are presented. The photometric evolution is characterised by rapidly-declining light curves ( $\Delta m_{15}(B)_{\text{true}} = 1.93$ ) and red colours at peak and soon thereafter. With  $M_{B,\text{max}} = -17.24$  the SN is an underluminous SN Ia, similar to the peculiar SNe 1991bg and 1999by. This similarity also holds for the spectroscopic appearance, the only remarkable difference being the likely presence of carbon in pre-maximum spectra of SN 2005bl. A comparison study among underluminous SNe Ia is performed, based on a number of spectrophotometric parameters. Previously reported correlations of the light-curve decline rate with peak luminosity and  $\mathcal{R}(\text{Si})$  are confirmed, and a large range of post-maximum Si II  $\lambda 6355$  velocity gradients is encountered. 1D synthetic spectra for SN 2005bl are presented, which confirm the presence of carbon and suggest an overall low burning efficiency with a significant amount of leftover unburned material. Also, the Fe content in pre-maximum spectra is very low, which may point to a low metallicity of the precursor. Implications for possible progenitor scenarios of underluminous SNe Ia are briefly discussed.

**Key words:** supernovae: general – supernovae: individual: SN 2005bl – supernovae: individual: SN 1991bg – supernovae: individual: SN 1999by – supernovae: individual: SN 1998de – galaxies: individual: NGC 4070.

## 1 INTRODUCTION

The history of underluminous SNe Ia is a typical example of the ever-recurring pattern in which knowledge about nature

\* Based on observations at ESO–Paranal, Prog. 075.D-0662(B)

† E-mail: tauben@mpa-garching.mpg.de

is accumulated. Usually, in the beginning there is the observation of a phenomenon, followed by a successful theoretical explanation. However, as further experiments or observations are carried out in order to confirm the newly developed theoretical ideas, often an ever higher degree of diversity and ever more exceptions from the simple rules are found the closer the subject of interest is studied. The need for refined and more complex theories to obtain a realistic description of the involved processes becomes evident.

In the case of SNe Ia, first a class of cosmic explosions apparently similar in absolute luminosity (“standard candles”) and spectroscopic appearance was identified. These events were explained as the disruptions of white dwarfs which had accreted matter until they reached their stability limit close to the Chandrasekhar mass ( $M_{\text{Ch}}$ ). However, in 1991 the paradigm of SN Ia homogeneity had to be relaxed a lot. This was triggered by the observation of two peculiar SNe Ia, which thereafter served as prototypes of newly-defined SN Ia subclasses with distinct spectrophotometric properties. One of these, SN 1991T (Filippenko et al. 1992a; Phillips et al. 1992; Ruiz-Lapuente et al. 1992; Mazzali, Danziger & Turatto 1995), was up to 0.6 mag brighter than average SNe Ia, and characterised by a hot early-time spectrum with strong Fe III features and weak or absent Si II and S II lines. The other one, SN 1991bg (Filippenko et al. 1992b; Leibundgut et al. 1993; Ruiz-Lapuente et al. 1993; Turatto et al. 1996; Mazzali et al. 1997) was even more deviant, with low ejecta velocities and a cool spectrum dominated by intermediate-mass-element (IME) lines and particularly strong O I and Ti II. Moreover, it had unusually red colours at early phases, and was underluminous by about 2 mag at peak (hereafter we will refer to such appearance as 91bg-like). Hence, quasi instantaneously the luminosity range of SNe Ia had increased to a factor of ten between the brightest and the faintest objects, proving that they were *no* standard candles. However, two years later Phillips (1993) realised a tight correlation between peak luminosity and decline rate in the *B* band. This relation and revised versions of it (e.g. Phillips et al. 1999) turned SNe Ia into standardisable candles, and hence made them an extremely useful tool for precision cosmology<sup>1</sup>.

In the following years, several more 91bg-like SNe Ia were discovered, but the available data set grew much less rapidly than for ordinary SNe Ia. From the results of the Lick Observatory Supernova Search (LOSS) and the Beijing Astronomical Observatory Supernova Survey (BAOSS), Li et al. (2001) estimated that about 16% of all SNe Ia are of the 91bg-like variety. This may still be an underestimate, as their low intrinsic luminosity makes 91bg-like SNe prone to Malmquist bias; nevertheless Li et al. (2001) estimated this effect to be negligible in their sample. Statistical studies (Hamuy et al. 1996a, 2000; Howell 2001) have shown that SNe Ia occur in all host-galaxy types, but revealed a correlation between SN decline rate and host morphology, with

a clear tendency for 91bg-like SNe to be associated with early-type hosts and hence old stellar populations.

While the single-degenerate (SD) Chandrasekhar-mass model has survived as the favoured scenario for the normal and indeed rather homogeneous SNe Ia, a number of alternative models have been suggested for the 91bg-like subclass. Ideas include double-degenerate (DD) explosions of merging white dwarfs, sub-Chandrasekhar-mass explosions triggered by detonation of the accreted helium layer (cf. Hillebrandt & Niemeyer 2000, for a review), and deflagrations in strongly rotating white dwarfs, where the turbulent propagation of the flame front is suppressed by the differential rotation (Pfannes 2006). Still, the notion that 91bg-like SNe are – in terms of the underlying explosion model – no different from ordinary SNe Ia, and that the only discriminating parameter is the mass of synthesised <sup>56</sup>Ni, has supporters in the SN Ia community. No conclusive evidence for any of these ideas has been found so far.

In this paper we present the joint data set of SN 2005bl obtained by the European Supernova Collaboration (ESC)<sup>2</sup> and the Carnegie Supernova Project (CSP)<sup>3</sup>. Since these observations are among the earliest ever obtained for a 91bg-like SN, they may help to better constrain possible progenitor and explosion models. The observations and techniques applied for data reduction and calibration are discussed in Section 2. In Section 3 we estimate the distance of SN 2005bl and the extinction along the line of sight. Sections 4 and 5 are devoted to the analysis of the light curves and spectra, respectively. Results of 1D spectrum synthesis calculations are presented in Section 6, and a comparison with other underluminous SNe Ia is performed in Section 7, where we also discuss the impact of SN 2005bl on our picture of SN Ia explosions. A short summary of the main results is given in Section 8.

## 2 OBSERVATIONS AND DATA REDUCTION

SN 2005bl ( $z = 0.024$ ) was discovered in the course of the Lick Observatory Supernova Search programme (LOSS) with the Katzman Automatic Imaging Telescope (KAIT) on UT 2005 April 14.34 and 15.36 at unfiltered magnitudes of 18.8 and 18.3, respectively (Shimasaki & Li 2005). The SN was not detected on images obtained with the same setup on UT 2005 March 11.33 to a limiting magnitude of 19.5. Based on spectra taken with the Las Campanas 2.5 m du Pont Telescope (+ WFCCD spectrograph) and the Fred Lawrence Whipple Observatory 1.5 m Telescope (+ FAST), SN 2005bl was classified as SN Ia, probably belonging to the 91bg-like variety given the similarity of the spectra with those of SN 1999by a few days before maximum light (Morrell et al. 2005; Gallagher et al. 2005a). The SN is located in the elliptical galaxy NGC 4070 (de Vaucouleurs morphological type –4.9; LEDA<sup>4</sup>), projected on a region of steep yet smooth background variation (Fig. 1). Details on the SN and host galaxy properties are summarised in Table 1.

<sup>1</sup> Several years later even more peculiar objects such as SN 2002cx (Li et al. 2003) were discovered which did not obey the Phillips relation, showing that not *all* SNe Ia are standardisable.

<sup>2</sup> <http://www.mpa-garching.mpg.de/~rtn/>

<sup>3</sup> <http://www.csp1.lco.cl/~cspuser1/PUB/CSP.html>

<sup>4</sup> Lyon-Meudon Extragalactic Database  
<http://leda.univ-lyon1.fr/>

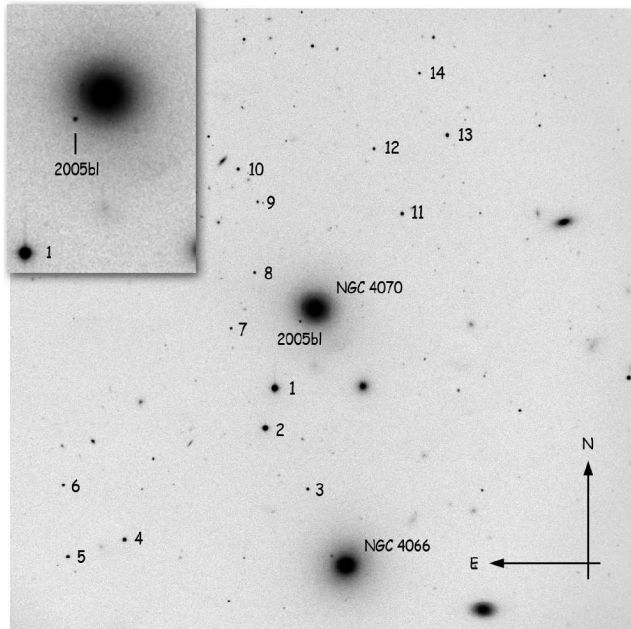


**Figure 1.** *R*-band image of the SN 2005bl field taken with the Calar Alto 2.2m Telescope + CAFOS on UT 2005 May 14. The field of view is  $9 \times 9$  arcmin<sup>2</sup>, and the local sequence stars are indicated. In the upper-left corner a twice-enlarged blow-up of the SN and its host galaxy is shown.

Although SN 2005bl was too distant to fulfil the formal selection criteria of the ESC, optical follow-up observations were performed owing to the peculiarities found in our first spectrum, obtained almost at the same time as the classification spectra by other groups. However, given the dimness of the SN, an intensive coverage as for other ESC targets was out of reach. In particular, the early part of the light curves was not well sampled owing to bad weather and scheduling constraints. At the same time, the CSP collaboration started their follow-up of SN 2005bl, focussing mainly on the photometric evolution near maximum light. Hence, the two data sets were almost perfectly complementary.

## 2.1 Photometric data

Optical photometry of SN 2005bl was acquired from one week before to about two months after maximum light in *B*. The basic data reduction (bias subtraction, overscan correction and flat-fielding) was performed using standard routines in IRAF<sup>6</sup> (Massey & Davis 1992; Massey 1997). The local sequence of stars in the SN field shown in Fig. 1 was calibrated with respect to a number of Landolt (1992, for *UBVRI*) and Sloan (Smith et al. 2002, for *ugriz*) standard fields on several photometric nights. The magnitudes of the calibrated local sequence, listed in Table 2, were used subsequently to determine the SN magnitudes in a relative measurement.

<sup>5</sup> NASA/IPAC Extragalactic Database  
<http://nedwww.ipac.caltech.edu/>

<sup>6</sup> IRAF is distributed by the National Optical Astronomy Observatories, which are operated by the Association of Universities for Research in Astronomy, Inc, under contract to the National Science Foundation.

**Table 1.** Properties of SN 2005bl and its host galaxy.

NGC 4059 / NGC 4070 <sup>a</sup>		
$\alpha$	12h04m11 <sup>s</sup> .43	1
$\delta$	+20°24′37″.7	1
redshift	$0.02406 \pm 0.00008$	2
recession velocity $v$	$7213 \pm 24$ km s <sup>-1</sup>	2
$v_{\text{Virgo}}^b$	$7330 \pm 28$ km s <sup>-1</sup>	2
$v_{\text{CMB}}^c$	$7534 \pm 33$ km s <sup>-1</sup>	2
distance modulus $\mu^d$	$35.10 \pm 0.09$ mag	2
apparent corr. <i>B</i> magnitude	$13.75 \pm 0.15$	1
morphological type <sup>e</sup>	E, -4.9	1
Galactic reddening $E(B-V)$	0.028 mag	3
SN 2005bl		
$\alpha$	12h04m12 <sup>s</sup> .32	4
$\delta$	+20°24′24″.8	4
offset from galaxy centre	13′.9 E, 11′.2 S	4
host reddening $E(B-V)$	$0.17 \pm 0.08$ mag	5
$\Delta m_{15}(B)_{\text{true}}$	$1.93 \pm 0.10$	5
JD <sub>max</sub> in <i>U</i>	$2\,453\,481.4 \pm 0.3$	5
JD <sub>max</sub> in <i>B</i>	$2\,453\,482.6 \pm 0.3$	5
JD <sub>max</sub> in <i>V</i>	$2\,453\,484.9 \pm 0.3$	5
JD <sub>max</sub> in <i>R</i>	$2\,453\,485.9 \pm 0.3$	5
JD <sub>max</sub> in <i>I</i>	$2\,453\,487.0 \pm 0.3$	5
JD <sub>max</sub> in <i>g</i>	$2\,453\,483.0 \pm 0.3$	5
JD <sub>max</sub> in <i>z</i>	$2\,453\,487.0 \pm 3.0$	5
$U_{\text{max}}$	$19.14 \pm 0.18$	5
$B_{\text{max}}$	$18.68 \pm 0.04$	5
$V_{\text{max}}$	$17.87 \pm 0.03$	5
$R_{\text{max}}$	$17.55 \pm 0.03$	5
$I_{\text{max}}$	$17.38 \pm 0.04$	5
$g_{\text{max}}$	$18.20 \pm 0.07$	5
$z_{\text{max}}$	$17.77 \pm 0.12$	5
$M_{U,\text{max}}$	$-16.91 \pm 0.43$	5
$M_{B,\text{max}}$	$-17.24 \pm 0.34$	5
$M_{V,\text{max}}$	$-17.85 \pm 0.27$	5
$M_{R,\text{max}}$	$-18.06 \pm 0.23$	5
$M_{I,\text{max}}$	$-18.10 \pm 0.18$	5
$M_{g,\text{max}}$	$-17.55 \pm 0.29$	5
$M_{z,\text{max}}$	$-17.67 \pm 0.20$	5

<sup>a</sup> The galaxy is listed twice in the NGC catalogue.

<sup>b</sup>  $v$  corrected for Local-Group infall onto Virgo cluster

<sup>c</sup>  $v$  corrected to the CMB reference frame

<sup>d</sup> from  $v_{\text{CMB}}$ , using  $H_0 = 72$  km s<sup>-1</sup>Mpc<sup>-1</sup>

<sup>e</sup> numerical code according to de Vaucouleurs

1: LEDA; 2: NED<sup>5</sup>; 3: Schlegel, Finkbeiner & Davis 1998; 4: Puckett & Langoussis 2005; 5: this work

For the sequence-star magnitudes in the Sloan *ugri* bands, the reader is referred to Contreras et al. (in prep.).

Although the host-galaxy background at the projected SN site seemed to be smooth, we applied the template-subtraction technique (Filippenko et al. 1986) in order to eliminate any possible contamination from the host galaxy, a justified concern given the faintness of the SN. For this purpose we acquired templates in *BVRI* with CAFOS mounted on the Calar Alto 2.2 m Telescope on UT 2006 March 28, and in *uBVgri* with the Las Campanas 2.5 m du Pont Telescope from UT 2006 April 3 to 30, about one year after the explosion when the SN had faded from visibility. For the ESC data, the galaxy subtraction was performed using the IRAF

**Table 2.** Magnitudes of the local sequence stars in the field of SN 2005bl (Fig. 1).

ID	<i>U</i>	<i>B</i>	<i>V</i>	<i>R</i>	<i>I</i>	<i>z</i>
1	15.207 ± 0.022	14.786 ± 0.013	13.952 ± 0.014	13.502 ± 0.010	13.080 ± 0.013	13.386 ± 0.013
2	16.387 ± 0.022	15.931 ± 0.012	15.048 ± 0.014	14.510 ± 0.011	14.011 ± 0.012	14.295 ± 0.024
3	18.340 ± 0.019	18.633 ± 0.021	18.110 ± 0.016	17.767 ± 0.013	17.385 ± 0.012	17.710 ± 0.074
4		18.154 ± 0.014	16.658 ± 0.020	15.665 ± 0.021	14.792 ± 0.017	
5		17.464 ± 0.009	16.962 ± 0.027	16.621 ± 0.007	16.269 ± 0.012	
6		19.132 ± 0.014	18.220 ± 0.015	17.690 ± 0.018	17.247 ± 0.010	
7	19.274 ± 0.017	19.488 ± 0.020	18.979 ± 0.014	18.629 ± 0.008	18.272 ± 0.015	18.526 ± 0.035
8	19.538 ± 0.022	19.396 ± 0.021	18.659 ± 0.019	18.251 ± 0.013	17.824 ± 0.017	18.096 ± 0.030
9	18.656 ± 0.049	18.924 ± 0.016	18.454 ± 0.018	18.115 ± 0.020	17.834 ± 0.018	18.112 ± 0.040
10		20.035 ± 0.020	18.640 ± 0.022	17.532 ± 0.014	16.260 ± 0.022	
11	18.355 ± 0.049	18.267 ± 0.013	17.539 ± 0.021	17.104 ± 0.015	16.687 ± 0.011	16.965 ± 0.014
12		18.346 ± 0.014	17.873 ± 0.020	17.510 ± 0.016	17.196 ± 0.011	
13		18.278 ± 0.011	17.206 ± 0.017	16.509 ± 0.018	15.893 ± 0.025	
14		19.083 ± 0.013	18.198 ± 0.023	17.666 ± 0.013	17.193 ± 0.020	

plug-in SVSUB written by S.V. (based on ISIS). The instrumental SN magnitudes were determined in the background-subtracted images with point-spread function (PSF) fitting photometry using the software package SNOOPY, specifically designed for this purpose by F. Patat and implemented in IRAF by E. Cappellaro. For the *z* band no templates were available, and the measurements were performed with ordinary background-fitting PSF photometry in SNOOPY. A check in the *BVRI* bands showed a good agreement between the two methods. Therefore, we are confident that also our *z*-band photometry is sufficiently reliable.

The calibration of the SN magnitudes to the desired standard photometric systems, the Johnson/Cousins system (Bessell 1990) for *UBVRI* and the Sloan system (Fukugita et al. 1996) for *g* and *z*, was complicated by the variety of filters mounted at the various telescopes, some of which deviated strongly from the standard. Fig. 2 shows the *BVRI* and *ri* response curves of all instruments used for the SN follow-up.

### Bessell photometry

In order to compensate for the differences in the transmission curves, and to report the magnitudes on the Bessell system, we made use of the “*S*-correction” technique based on the prescription of Stritzinger et al. (2002), Pignata et al. (2004), and references therein. *S*-corrections were computed for the *BVRI* and Sloan *ri* data, based on our spectra of SN 2005bl. Unfortunately, the spectra do not fully cover the *U*-band region, so that no *U*-band *S*-correction could be derived. Instead, transformation formulae (Jordi, Grebel & Ammon 2006; Zhao & Newberg 2006) were employed to convert the Swope *u*-band data to the Bessell system. Similarly, no *S*-correction was applied to data later than +50 d, since our spectroscopic follow-up ends already well before. The strong deviation of the MONICA *V* filter (actually a Roeser *BV* filter) from the Bessell description (see Fig. 2), along with some lacking information required to reconstruct the response curve, makes the MONICA *V*-band correction less reliable.

The redshift of SN 2005bl is not negligible. Therefore, in computing the *S*-correction the spectra were shifted in

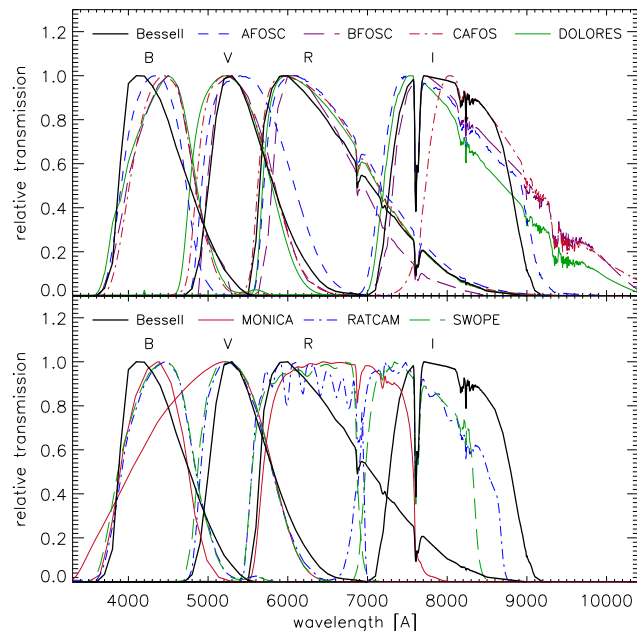


**Figure 2.** Instrumental *BVRI* / *ri* passbands used for the observations of SN 2005bl. The standard Bessell (1990) curves are also displayed in the figure for comparison.

order to account also for the *K*-correction. Since the same restrictions as before apply also here, no *K*-correction was performed for the *U* band and for any data later than +50 d.

In Table 3 the fully calibrated and – whenever possible – *S*- and *K*-corrected *UBVRI* Bessell magnitudes of SN 2005bl are reported, together with their uncertainties. Both the intrinsic Bessell data and the transformed Sloan photometry entered into this Table. Table 4 shows the combined *S*- and *K*-correction, i.e., the difference between the magnitudes of Table 3 and those obtained with a first-order colour-term calibration. The differences are significant, so that the lack of the *S*- and *K*-correction for *U* may introduce considerable uncertainties.

**Table 3.** *S*- and *K*-corrected Bessell magnitudes of SN 2005bl.<sup>a</sup>

JD <sup>b</sup>	Epoch <sup>c</sup>	<i>U</i>	<i>B</i>	<i>V</i>	<i>R</i>	<i>I</i>	Telescope	Seeing <sup>d</sup>
476.61	-6.0	19.591 ± 0.114	19.364 ± 0.022	18.950 ± 0.030	18.776 ± 0.024	18.599 ± 0.045	SWO	1.41
477.63	-5.0	19.389 ± 0.117	19.135 ± 0.022	18.695 ± 0.029	18.523 ± 0.023	18.402 ± 0.038	SWO	1.34
478.66	-3.9	19.237 ± 0.134	18.955 ± 0.022	18.461 ± 0.029	18.290 ± 0.022	18.120 ± 0.036	SWO	1.68
479.64	-3.0		18.818 ± 0.029	18.307 ± 0.031	18.116 ± 0.030	17.948 ± 0.043	SWO	1.57
479.68	-2.9			18.393 ± 0.042	18.120 ± 0.030	17.883 ± 0.034	TNG	1.47
480.65	-1.9	19.151 ± 0.144	18.766 ± 0.025	18.150 ± 0.029	17.883 ± 0.028	17.770 ± 0.038	SWO	1.44
481.61	-1.0	19.185 ± 0.174	18.709 ± 0.027	18.052 ± 0.030	17.798 ± 0.022	17.650 ± 0.036	SWO	1.45
483.62	1.0	19.235 ± 0.203	18.682 ± 0.040	17.899 ± 0.030	17.636 ± 0.026	17.513 ± 0.039	SWO	1.54
484.65	2.1	19.296 ± 0.291	18.733 ± 0.042	17.839 ± 0.031	17.526 ± 0.043	17.414 ± 0.045	SWO	1.52
485.39	2.8		18.872 ± 0.036	17.887 ± 0.051	17.563 ± 0.035	17.361 ± 0.051	LT	0.84
489.32	6.7			18.172 ± 0.280			WD	1.89
489.59	7.0	20.248 ± 0.152	19.472 ± 0.031	18.146 ± 0.027	17.692 ± 0.021	17.416 ± 0.035	SWO	1.84
490.52	7.9	20.640 ± 0.155	19.653 ± 0.026	18.194 ± 0.025	17.781 ± 0.025	17.435 ± 0.044	LT	0.81
490.60	8.0	20.640 ± 0.163	19.687 ± 0.023	18.258 ± 0.028	17.791 ± 0.022	17.456 ± 0.038	SWO	1.34
491.51	8.9		19.824 ± 0.046	18.296 ± 0.048	17.845 ± 0.027		WD	1.60
491.57	9.0	20.620 ± 0.140	19.834 ± 0.022	18.359 ± 0.029	17.836 ± 0.026	17.477 ± 0.039	SWO	1.37
493.35	10.8			18.553 ± 0.028	17.959 ± 0.025	17.503 ± 0.031	LOI	2.41
498.38	15.8				18.551 ± 0.045	17.805 ± 0.052	LT	0.95
500.51	17.9			19.258 ± 0.184	18.722 ± 0.041		WD	2.38
502.38	19.8				18.807 ± 0.034	18.192 ± 0.063	LT	0.70
503.35	20.8		20.912 ± 0.073	19.334 ± 0.040	18.960 ± 0.023		WD	1.55
503.35	20.8		20.893 ± 0.133	19.429 ± 0.046	18.965 ± 0.074	18.361 ± 0.059	Ekar	2.57
504.49	21.9				19.035 ± 0.035	18.325 ± 0.057	LT	0.67
505.49	22.9		20.936 ± 0.050	19.609 ± 0.069	19.180 ± 0.045	18.474 ± 0.064	Caha	1.29
506.41	23.8		21.052 ± 0.081	19.597 ± 0.037	19.216 ± 0.028	18.571 ± 0.035	Caha	1.91
510.53	27.9			19.693 ± 0.119			WD	1.70
511.36	28.8			19.687 ± 0.092	19.530 ± 0.045		WD	1.70
512.55	29.9		21.168 ± 0.176	19.847 ± 0.063	19.480 ± 0.036	18.874 ± 0.051	SWO	1.56
516.48	33.9				19.877 ± 0.073		WD	1.78
518.43	35.8			20.044 ± 0.068	20.020 ± 0.042		WD	1.52
519.40	36.8		21.421 ± 0.075	20.031 ± 0.042	19.925 ± 0.055	19.310 ± 0.096	LT	1.01
520.44	37.8		21.407 ± 0.124	20.205 ± 0.055	20.002 ± 0.045		WD	2.07
521.39	38.8			20.122 ± 0.040	20.009 ± 0.036	19.358 ± 0.094	LT	0.96
524.42	41.8		21.379 ± 0.097	20.141 ± 0.069	20.159 ± 0.071		WD	1.40
538.38	55.8			20.685 ± 0.168			WD	1.75
548.41	65.8			20.984 ± 0.280	21.183 ± 0.347		WD	2.15

<sup>a</sup> No *S*- and *K*-correction applied in the *U* band and to any data after +50 d. <sup>b</sup> JD - 2 453 000.00 <sup>c</sup> Epoch in days with respect to the *B*-band maximum JD 2 453 482.6 ± 0.5. <sup>d</sup> Average seeing in arcsec over all filter bands.

SWO = Las Campanas 1.0m Swope Telescope + CCD; <http://www.lco.cl/telescopes-information/henrietta-swope/>  
TNG = 3.58 m Telescopio Nazionale Galileo + DOLORES; <http://www.tng.iac.es/instruments/lrs/>  
LT = 2.0 m Liverpool Telescope + RATCAM; <http://telescope.livjm.ac.uk/Info/TelInst/Inst/RATCam/>  
WD = 0.8 m Wendelstein Telescope + MONICA; <http://www.wendelstein-observatorium.de/monica/monica-en.html>  
LOI = 1.52 m Loiano Telescope + BFOSC; <http://www.bo.astro.it/loiano/152cm.html>  
Ekar = Asiago 1.82 m Telescope + AFOSC; <http://www.oapd.inaf.it/asiago/2000/2300/2310.html>  
Caha = Calar Alto 2.2 m Telescope + CAFOS SiTe; <http://www.caha.es/CAHA/Instruments/CAFOS/>

## Sloan photometry

Besides transforming the Swope and Liverpool Sloan-filter observations to the Bessell system via *S*-corrections, light curves in the Sloan photometric system itself were constructed. The magnitudes were calibrated through first-order colour equations without employing *S*-corrections, since at both telescopes the filters are close to the standard Sloan prescription. Table 5 reports the Sloan *griz* photometry from the Liverpool telescope. For the original Swope photometry see Contreras et al. (in prep.).

## 2.2 Spectroscopic data

Details of the spectroscopic observations of SN 2005bl are reported in Table 6. All two-dimensional spectroscopic frames were first debiased and flat-fielded, before an optimal, variance-weighted extraction of the spectra (Horne 1986; Massey, Valdes & Barnes 1992) was performed using the IRAF routine APALL. Wavelength calibration was accomplished with the help of arc-lamp exposures or, whenever this was not possible, using the night-sky lines. The instrumental response functions required for flux calibration were determined from observations of the spectrophotometric standard stars reported in Table 6. Whenever no standard had been observed, the sensitivity curve obtained on

**Table 5.** Sloan photometry of SN 2005bl obtained with the Liverpool telescope. No *S*- and *K*-correction has been applied. For the Swope data see Contreras et al. (in prep.).

JD <sup>a</sup>	Epoch <sup>b</sup>	<i>g</i>	<i>r</i>	<i>i</i>	<i>z</i>
485.4	2.8	18.295 ± 0.115	17.669 ± 0.023	17.866 ± 0.051	17.769 ± 0.080
490.5	7.9		17.877 ± 0.025	17.870 ± 0.031	17.808 ± 0.039
498.4	15.8		18.676 ± 0.046	18.308 ± 0.092	18.113 ± 0.080
502.4	19.8		18.921 ± 0.039	18.760 ± 0.059	
504.5	21.9		19.138 ± 0.047	18.878 ± 0.077	18.548 ± 0.095
519.4	36.8		19.998 ± 0.071	19.982 ± 0.093	19.548 ± 0.165
521.4	38.8		20.073 ± 0.043	20.081 ± 0.100	19.680 ± 0.240

<sup>a</sup> JD − 2 453 000.0    <sup>b</sup> Epoch in days with respect to *B*-band maximum (JD = 2 453 482.6 ± 0.5).

**Table 6.** Journal of spectroscopic observations of SN 2005bl.

UT Date	JD <sup>a</sup>	Epoch <sup>b</sup>	Exposure	Airmass	Tel.	Grism	Range [Å]	Res. [Å] <sup>c</sup>	Standards
05/04/16	476.6	−6.0	900 s × 3	1.54	DUP	blue	3800 − 9200	6	L745-46A, LTT7987
05/04/17	477.6	−5.0	2400 s	1.54	Caha	b200	3500 − 8800	10	BD+33 2642
05/04/19	479.6	−3.0	900 s × 3	1.54	DUP	blue	3700 − 9000	6	L745-46A, LTT7379
05/04/19	479.7	−2.9	1200 s	2.06	TNG	LR-R	5000 − 9750	11	H <sub>z</sub> 44
05/04/26	487.4	4.8	1500 s	1.09	TNG	LR-B	3300 − 8000	13	Feige 34
05/04/26	487.4	4.8	1500 s	1.15	TNG	LR-R	5000 − 9750	12	Feige 34
05/05/04	495.5	12.9	1500 s	1.04	TNG	LR-B	3500 − 8900	14	Feige 56
05/05/04	495.5	12.9	1500 s	1.08	TNG	LR-R	5000 − 9750	12	Feige 56
05/05/11	502.4	19.8	1500 s × 2	1.01	TNG	LR-B	3300 − 8000	14	Feige 66
05/05/11	502.4	19.8	2700 s × 2	1.14	Caha	r200	6200 − 9750	11	Feige 34
05/05/14	505.4	22.8	2400 s × 2	1.11	Caha	b200	3500 − 8800	14	BD+33 2642
05/05/24	515.6	33.0	1800 s	1.93	VLT	300V + GG375	4200 − 9600	9	LTT7987

<sup>a</sup> JD − 2 453 000.0    <sup>b</sup> Relative to *B*-band maximum (JD = 2 453 482.6 ± 0.5).    <sup>c</sup> Full-width at half maximum (FWHM) of isolated, unblended night-sky lines.

DUP = Las Campanas 2.5 m du Pont Telescope + WFCCD; <http://www.lco.cl/telescopes-information/irenee-du-pont/>

Caha = Calar Alto 2.2 m Telescope + CAFOS SiTe; <http://www.caha.es/CAHA/Instruments/CAFOS/>

TNG = 3.58 m Telescopio Nazionale Galileo + DOLORES; <http://www.tng.iac.es/instruments/lrs/>

VLT = ESO 8.2 m Very Large Telescope UT1 + FORS2; <http://www.eso.org/instruments/fors2/>

a different night with the same instrumental configuration was used. Atmospheric extinction correction was applied using tabulated extinction coefficients for each telescope site. Telluric features were identified in the spectra of the spectrophotometric standard stars and removed from the SN spectra. To check the calibration, the spectroscopic fluxes were transformed into magnitudes by integrating the spectra convolved with Bessell (1990) filter functions. Whenever necessary, the spectral fluxes were adjusted to match the contemporaneous photometry. Finally, spectra of similar quality obtained during the same night were combined to increase the signal-to-noise ratio (S/N); if the wavelength range of these spectra was different, they were averaged in their overlap region.

As a consequence of charge-transfer-efficiency problems of the DOLORES CCD, it was not possible to remove the night-sky emission in the TNG spectra cleanly. A pattern of negative and positive residuals was left, sometimes at wavelengths coinciding with spectral features of the SN, thus limiting the reliability of line-depth measurements. To mitigate this problem, the lines affected were fitted with polynomials, excluding from the fit the regions of strongest residuals, and then the depth was determined in the polynomial curves.

### 3 DISTANCE, EXTINCTION AND HOST GALAXY PROPERTIES

Like most 91bg-like SNe Ia (Gallagher et al. 2005b), SN 2005bl exploded in an early-type host, the elliptical galaxy NGC 4070. Other prominent examples are SN 1991bg itself and SN 1997cn in elliptical hosts (Filippenko et al. 1992b; Leibundgut et al. 1993; Turatto et al. 1996, 1998), and SN 1998de whose host galaxy was of type S0 (Modjaz et al. 2001).<sup>7</sup> Since early-type galaxies are assumed to have experienced no significant star formation over long times, this behaviour might be indicative of 91bg-like SNe Ia originating from an old stellar population. Even if one allows for some more recent star formation in elliptical galaxies (e.g. triggered by mergers or interaction), the relative paucity of 91bg-like SNe in late-type, actively star-forming galaxies clearly disfavour young or intermediate-aged stellar progenitors or progenitor systems.

A widely accepted paradigm for elliptical galaxies is that they have only little interstellar gas and dust (but see

<sup>7</sup> SN 1999by (Garnavich et al. 2004) was hosted by NGC 2841, a spiral galaxy, but with the spectral appearance of an elliptical galaxy (Gallagher et al. 2005b).

**Table 4.** Amount of  $S$ - and  $K$ -correction contained in the magnitudes reported in Table 3. No  $S$ - and  $K$ -correction has been applied to the  $U$ -band data.

JD <sup>a</sup>	Epoch <sup>b</sup>	$B$	$V$	$R$	$I$	Tel. <sup>c</sup>
476.6	-6.0	-0.020	0.030	0.033	0.147	SWO
477.6	-5.0	-0.038	0.029	0.044	0.177	SWO
478.7	-3.9	-0.028	0.011	0.045	0.162	SWO
479.6	-3.0	-0.054	0.011	0.044	0.151	SWO
479.7	-2.9		0.123	0.193	0.252	TNG
480.7	-1.9	-0.032	0.007	0.022	0.093	SWO
481.6	-1.0	-0.062	-0.003	0.043	0.110	SWO
483.6	1.0	-0.078	-0.044	0.088	0.102	SWO
484.7	2.1	-0.099	-0.042	0.048	0.085	SWO
485.4	2.8	-0.077	-0.002	0.136	-0.054	LT
489.3	6.7		0.137			WD
489.6	7.0	-0.113	-0.039	0.187	0.060	SWO
490.5	7.9	-0.116	-0.034	0.166	-0.042	LT
490.6	8.0	-0.128	-0.065	0.213	0.049	SWO
491.5	8.9	-0.233	-0.034	0.074		WD
491.6	9.0	-0.142	-0.074	0.190	0.035	SWO
493.4	10.8		-0.029	0.027	-0.018	LOI
498.4	15.8			0.126	-0.105	LT
500.5	17.9		-0.064	0.096		WD
502.4	19.8			0.096	-0.209	LT
503.4	20.8	-0.237	-0.065	0.074		WD
503.4	20.8	-0.166	-0.067	0.055	-0.017	Ekar
504.5	21.9			0.113	-0.220	LT
505.5	22.9	-0.201	-0.087	0.083	0.009	Caha
506.4	23.8	-0.207	-0.085	0.093	0.011	Caha
510.5	27.9		-0.292			WD
511.4	28.8		-0.286	0.062		WD
512.6	29.9	-0.150	-0.084	0.199	-0.218	SWO
516.5	33.9			0.078		WD
518.4	35.8		-0.037	0.082		WD
519.4	36.8	-0.125	-0.038	0.120	-0.304	LT
520.4	37.8	-0.196	-0.076	0.076		WD
521.4	38.8		-0.078	0.127	-0.304	LT
524.4	41.8	-0.191	-0.054	0.074		WD

<sup>a</sup> JD - 2453 000.0 <sup>b</sup> Epoch in days with respect to the estimated  $B$ -band maximum JD 2453 482.6  $\pm$  0.5. <sup>c</sup> See Table 3 for details.

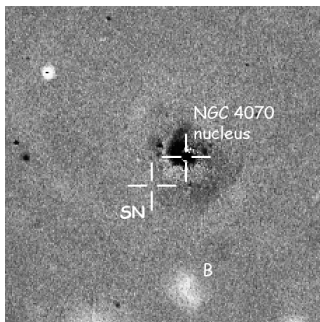


**Figure 3.**  $B - R$  difference image of NGC 4070, constructed as described in the text. Dark shades in the figure correspond to red areas. The field of view is  $2 \times 2$  arcmin<sup>2</sup>; north is up, east to the left. Crosshairs mark the explosion site of SN 2005bl and the centre of NGC 4070. ‘B’ denotes a bluish patch, probably a companion galaxy of NGC 4070 (see discussion in the text).

Patil et al. 2007 for a more sophisticated picture). This is consistent with the negligible host-galaxy extinction found in SNe 1991bg, 1997cn and 1998de. However, recent mergers or interaction may alter this picture, as exemplified by the radio galaxy Centaurus A, the host of SN 1986G (Phillips et al. 1987). In this case, the SN lay behind a prominent dust lane, and consequently was strongly extinguished. In NGC 4070 no such dust lane is visible even in deep images, but SN 2005bl showed signs of extinction within its host galaxy, the most prominent being a narrow interstellar Na I D line in the spectra at the redshift of the host, with an equivalent width (EW) of  $2.6 \pm 0.3 \text{ \AA}$ .

Since elliptical galaxies lack H II regions with strong emission lines, their surface colours are good tracers of the internal dust distribution (Patil et al. 2007). Hence, to investigate the dust content in NGC 4070, we constructed a  $B - R$  image of the galaxy from the templates obtained with CAFOS on UT 2006 March 28, following largely the prescription of Patil et al. (2007): after the usual pre-reduction, the  $B$ - and  $R$ -band images were spatially aligned, and the sky background was subtracted. The images were then scaled to contain the same flux inside an aperture of 45 arcsec around the centre of NGC 4070, and subtracted one from the other. The difference image is shown in Fig. 3. Both the centre of the galaxy and the position of SN 2005bl are marked. Dark shades correspond to redder areas, indicative of either dust or an intrinsically redder stellar population. A red region is present to the immediate east and north-east of the nucleus, and another more extended but less opaque arc to its south-west. This asymmetric surface-colour distribution suggests that there probably is dust in NGC 4070. However, at the exact position of SN 2005bl no major blue or red structures can be discerned, so that the dust obscuring the SN is probably too locally confined to be resolved.

Deep images of NGC 4070 reveal some deviation from a perfectly spherical or ellipsoidal shape (Fig. 4). This is an indication of fairly recent interaction, either with the galaxy 2MASX J12040831+2023280 about 1.3 arcmin to its south-west (labelled ‘A’ in Fig. 4), or with a small knot about 0.8 arcmin to its south (labelled ‘B’, and most easily seen as irregularly-shaped bright patch in the lower part of Fig. 3). Furthermore, in Fig. 4 a faint, broad bridge of luminous matter between NGC 4070 and its equally massive elliptical neighbour galaxy NGC 4066 can be detected.<sup>8</sup> The two galaxies are offset by about 3.74 arcmin, which corresponds to a projected distance of 114 kpc (for  $H_0 = 72 \text{ km s}^{-1} \text{ Mpc}^{-1}$ ).

The exact amount of dust extinction towards SN 2005bl is quite difficult to determine, and it constitutes the main uncertainty in the calibration of the SN absolute magnitudes. The Galactic component is small, with a colour excess  $E(B - V) \approx 0.03 \text{ mag}$  (Schlegel et al. 1998). However, as mentioned before, the contribution of dust in the host galaxy is significant. With  $\text{EW}(\text{Na I D}) = 2.6 \pm 0.3 \text{ \AA}$  and applying

$$E(B - V) = 0.16 \times \text{EW}(\text{Na I D}),$$

(Turatto, Benetti & Cappellaro 2003), we obtain  $E(B -$

<sup>8</sup> The situation is somewhat reminiscent of SN Ia 2005cf (Pastorello et al. 2007a), with the difference that this SN was directly located in the tidal bridge.

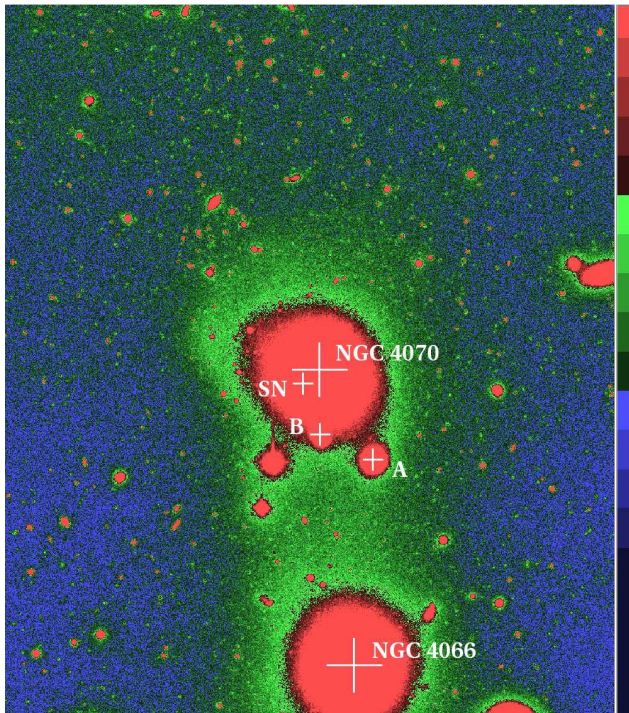


**Figure 4.** Deep  $7.7 \times 9.0$  arcmin<sup>2</sup> exposure of NGC 4070 and its neighbour NGC 4066 obtained on UT 2006 March 28 with CAFOS. North is up, east to the left; brightness increases from blue over green to red. The distorted shape of NGC 4070 and the bridge of luminous matter connecting the two galaxies are discernible. ‘A’ and ‘B’ mark companion galaxies of NGC 4070.

$V)_{\text{host}} = 0.42 \pm 0.05$  mag. However, the lack of knowledge of the extinguishing material’s gas-to-dust ratio makes this method very uncertain. Therefore, in the case of Type Ia SNe, alternative ways to determine the colour excess using the light and colour curves are usually preferred. Among the most well-known is the Lira (1995) relation, which assumes a uniform  $B - V$  colour evolution of SNe Ia between 30 and 90 d after maximum (but see Wang et al. 2007 for a recent warning about the use of this method). Apparently, this relation seems to hold also for underluminous SNe Ia, which are characterised by much redder  $B - V$  colours at maximum and soon thereafter. However, the decreasing quality of the SN 2005bl photometry after +30 d and the lack of  $B$ -band observations later than +42 d, result in a relatively large range of colour excesses consistent with the Lira relation, from  $E(B - V)_{\text{host}} \approx 0.12$  to 0.25 mag.

Since SN 2005bl is an underluminous SN Ia with  $\Delta m_{15}(B)_{\text{true}} = 1.93$  (cf. Section 4.1), SNe 1991bg and 1999by ( $\Delta m_{15}(B)_{\text{true}} = 1.94$  and 1.90, respectively; cf. Section 7) are natural comparison objects. Despite their numerous similarities, the reddening-corrected colour curves of the two latter objects differ especially at early phases, SN 1991bg being  $\sim 0.15$  mag redder in  $B - V$  than SN 1999by. This intrinsic colour difference directly propagates to an uncertainty in the inferred colour excess of SN 2005bl determined on the basis of such comparison. Matching the colours of SN 2005bl to SN 1991bg, we obtain  $E(B - V)_{\text{host}} \approx 0.13 \pm 0.05$  mag, whereas a comparison with SN 1999by yields  $E(B - V)_{\text{host}} \approx 0.29 \pm 0.05$  mag.

A study of the extinction law towards SN 2005bl, analo-

gous to that presented by Elias-Rosa et al. (2006) and based on extracting an extinction curve from a comparison with coeval spectra of SNe 1991bg and 1999by, yields a host-galaxy colour excess of  $0.22 \pm 0.02$  mag. Furthermore, no deviation of the total-to-selective-extinction parameter  $R_V$  from the canonical value of 3.1 as inferred from “standard” dust in the Milky Way can be discerned.

For the rest of the discussion we assume  $E(B - V)_{\text{host}} = 0.17 \pm 0.08$  mag. This estimate is based solely on the study of the SN colours (giving the strongest weight to the comparison with SN 1991bg), and ignores the larger colour-excess estimate from the interstellar NaID line, since the latter would result in too blue a colour and too high an absolute luminosity given SN 2005bl’s spectrophotometric similarity to SNe 1991bg and 1999by. This choice of  $E(B - V)_{\text{host}}$ , together with the foreground reddening of 0.03 mag, yields a total colour excess  $E(B - V)_{\text{total}} = 0.20 \pm 0.08$  mag and, adopting a standard Cardelli, Clayton & Mathis (1989) reddening law with  $R_V = 3.1$ , a total  $B$ -band extinction along the line of sight of  $A_B = 0.82 \pm 0.33$  mag.

With a recession velocity corrected to the CMB reference frame of  $7534 \pm 33$  km s<sup>-1</sup> (Table 1), NGC 4070 is well within the Hubble flow. Adopting  $H_0 = 72$  km s<sup>-1</sup>Mpc<sup>-1</sup> (Freedman et al. 2001; Spergel et al. 2003), this corresponds to a distance of 104.6 Mpc and a kinematical distance modulus  $\mu = 35.10$  mag, similar to that of the Coma Cluster. However, the latter is about  $14^\circ 45'$  away (which, at the given distance, corresponds to 27 Mpc), excluding any physical association. Accounting for an uncertainty of 300 km s<sup>-1</sup> arising from a possible peculiar motion of NGC 4070, we obtain  $\mu = 35.10 \pm 0.09$  mag.

## 4 PHOTOMETRIC EVOLUTION

### 4.1 Filtered light curves

The photometric observations of SN 2005bl are among the earliest ever obtained for a 91bg-like SN. In Fig. 5 we present the Bessell  $UBVRI$  and Sloan  $gz$  light curves, i.e. the data of Tables 3 and 5, and Contreras et al. (in prep.).  $S + K$ -corrections have been applied to the  $BVRI$  bands. Also shown are  $BVI$ -templates constructed from SN 1991bg (Hamuy et al. 1996c), reddened by  $E(B - V) = 0.20$  mag. These provide an excellent match to SN 2005bl.

Compared to normal-luminosity SNe Ia the light curves of SN 2005bl are characterised by a fast rise to and decline from the light-curve peak, especially in the blue bands. Moreover, in the  $B$  band the settling to the exponential tail (corresponding to the bend parameter  $t_b$  of Pskovskii 1984 and the intersection parameter  $t_2^B$  as defined by Hamuy et al. 1996c) occurs at a remarkably early epoch, only about 15 d after maximum, as compared to 25–38 d for intermediate and slow decliners (Hamuy et al. 1996c). Consequently, the decline from the peak to the onset of the radioactive tail is only  $\sim 1.9$  mag, less than in most SNe Ia with shallower initial decline.

The exact value of the Phillips (1993) decline rate parameter  $\Delta m_{15}(B)$  is difficult to measure directly because of a gap in the light curves around +15 d. A polynomial fit including the  $B$ -band data up to one month past maximum yields  $\Delta m_{15}(B) = 1.91$ , and we adopt a conservative error

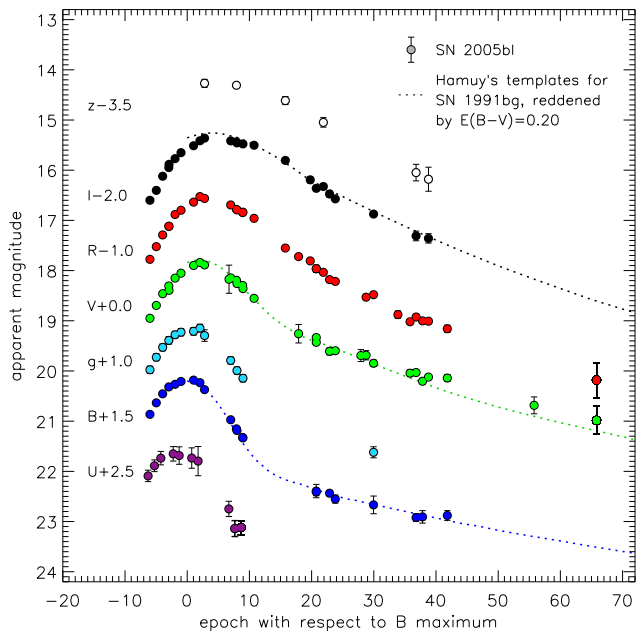


**Figure 5.** *UBVRIZ* Bessell and *gz* Sloan light curves of SN 2005bl. The *BVRIZ* data (Table 3) are *S*- and *K*-corrected except for the latest phases, while the *U*, *g* and *z* data (Tables 3, 5 and Contreras et al. in prep.) are not. Hamuy et al.’s (1996c) templates for SN 1991bg are shown for comparison (dotted lines).

of 0.10 to account for the fact that the fit around +15 d is not very well constrained. After correction for the mitigating effects of extinction (Phillips et al. 1999) this turns into an actual decline rate  $\Delta m_{15}(B)_{\text{true}} = 1.93 \pm 0.10$ .

Besides the *B* band, differences with respect to normal-luminosity SNe Ia are most pronounced in the near-IR (*I* and *z* bands), where – like in other 91bg-like SNe – the secondary light-curve maximum is absent, and the main maximum is delayed with respect to that in *B* (JD 2453482.6  $\pm$  0.5) by a couple of days rather than advanced. In general, the instance of peak brightness seems to be the more delayed the redder the band is. *V*-band maximum occurs 2.3 d after that in *B*, and those in *R* and *I* are delayed by 3.3 and 4.4 d, respectively (see Table 1), whereas in *U* the light-curve peak precedes that in *B* by about 1.0 d. For the *z* band the sparse photometric coverage does not allow for an exact determination of the time of maximum light, but it can be estimated to be similarly delayed as in *R* or *I*.

The absolute peak magnitudes of SN 2005bl (Table 1), calculated adopting the distance and extinction estimates presented in Section 3, reveal that the SN is underluminous by 1 to 2 mag in all filters compared to a canonical,  $\Delta m_{15}(B)_{\text{true}} = 1.1$  SN Ia, the difference being most pronounced in the blue bands.

## 4.2 Bolometric light curve

The differences in luminosity can clearly be seen in Fig. 6, where the quasi-bolometric light curve of SN 2005bl is compared to those of the other underluminous SNe Ia 1991bg, 1997cn, 1998de and 1999by (Filippenko et al. 1992b; Leibundgut et al. 1993; Turatto et al. 1996, 1998; Modjaz et al. 2001; Garnavich et al. 2004), and the in-

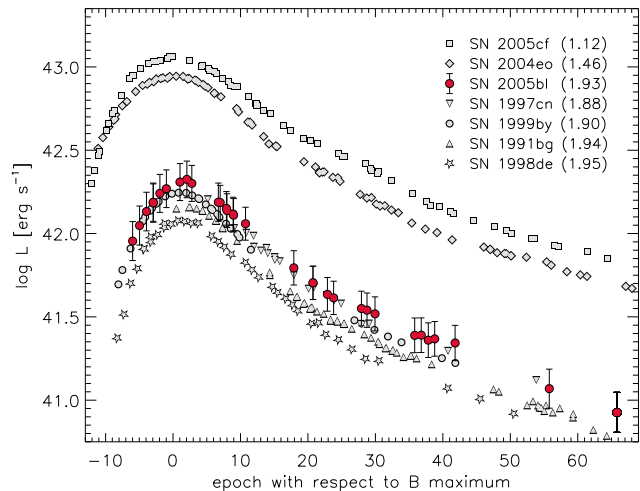


**Figure 6.** Quasi-bolometric light curves of SNe 2005bl, 1991bg, 1997cn, 1998de, 1999by, 2004eo and 2005cf, obtained by integrating the *U*-through-*I*-band fluxes (for the adopted distance and extinction parameters see Table 8 and Pastorello et al. 2007a,b). Error bars are shown for SN 2005bl only, and account for uncertainties in the photometric calibration, distance and extinction estimates. The  $\Delta m_{15}(B)_{\text{true}}$  of the SNe is given in parentheses.

termediate decliner SN Ia 2004eo ( $\Delta m_{15}(B)_{\text{true}} = 1.46$ , Pastorello et al. 2007b), which forms a bridge to canonical, normal-luminosity SNe Ia such as 2005cf ( $\Delta m_{15}(B)_{\text{true}} = 1.12$ , Pastorello et al. 2007a). The integrated optical light curves (see, e.g., Nomoto, Filippenko & Shigeyama 1990) were constructed in the following way: in a first step the *U*-through-*I* magnitudes were converted to monochromatic fluxes and the spectral energy distribution (SED) was interpolated linearly. The SED was then integrated over frequency, assuming zero flux at the integration limits, which are given by the blue edge of the *U* band and the red edge of the *I* band. Whenever no *U*-band observations were available, or the coverage of this band was incomplete, a correction derived from SN 1999by was applied to the analogously constructed *B*-through-*I* light curve. This method appeared more reliable than applying *U*-band corrections based on ordinary SNe Ia.

As Fig. 6 shows, 91bg-like SNe form a fairly homogeneous group in terms of bolometric light-curve shape and luminosity. Both their light-curve width and their luminosities distinguish them even from intermediate decliners such as SN 2004eo. SNe Ia with  $\Delta m_{15}(B)_{\text{true}} \sim 1.50$ – $1.85$  (which are rare, cf. Section 7.1) would probably fall in the gap between SN 2004eo and the 91bg-like SNe. In Fig. 6 they are not included because their light-curve coverage is insufficient in some of the relevant bands. Within the 91bg-like group, SN 2005bl appears to be the brightest object ( $\log L_{\text{max}} = 42.31 \pm 0.11$ ), but the differences are mostly within the error bars, which for SN 2005bl are dominated by the uncertainty in the host-galaxy extinction.

In the only rapidly-declining SN Ia with extended near-IR photometry, SN 1999by (Höflich et al. 2002; Garnavich et al. 2004)<sup>9</sup>, the *JHK* bands contribute  $\sim 25\%$  to the total bolometric flux around maximum, and  $\sim 36\%$

<sup>9</sup> SN 1991bg has been observed in *JHK* by Porter et al. (1992)

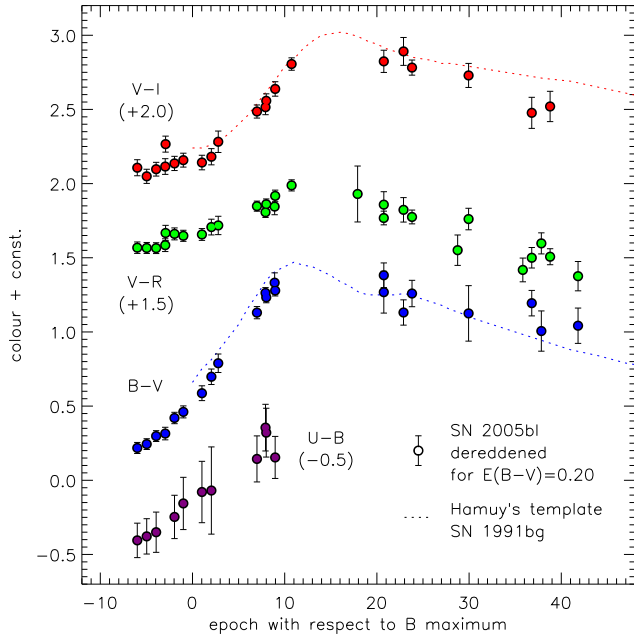


**Figure 7.** Time-evolution of the  $U - B$ ,  $B - V$ ,  $V - R$  and  $V - I$  colour indices of SN 2005bl. The curves have been reddening-corrected adopting a Cardelli et al. (1989) extinction law with  $E(B - V) = 0.20$  mag and  $R_V = 3.1$ .

after one month. The corresponding numbers measured for SN 2004eo are  $\sim 16\%$  and  $\sim 37\%$ , respectively. This means that at early phases the near IR gives a larger contribution in the fast decliners than it does in intermediate and slow decliners, but that by +30d the difference has vanished. Wavelength regions other than the optical and near-IR appear to contribute very little to the total bolometric flux in SNe Ia (Suntzeff 1996; Contardo, Leibundgut & Vacca 2000). Therefore, neglecting these regimes should not cause a significant underestimate of the true bolometric luminosity.

### 4.3 Colour evolution

Fig. 7 presents the time-evolution of the  $U - B$ ,  $B - V$ ,  $V - R$  and  $V - I$  colours of SN 2005bl. The good agreement with the colour curves of SN 1991bg (Hamuy et al. 1996c) also shown in the figure is evident. Except for the late  $V - R$  points, all colour indices are  $> 0$  throughout the investigated period, indicating that SN 2005bl – like other rapidly-declining SNe Ia – was a rather red event. In particular it was much redder at early phases than ordinary SNe Ia, which are characterised by a  $B - V$  between 0.0 and  $-0.1$  at maximum light. Remarkably, the evolution of SN 2005bl's various colour indices with time is very similar. From our first observations at  $-6$  d on, all colours become monotonically redder until at least  $\sim 10$  d after maximum, and almost simultaneously exhibit a red peak between +12 and +17 d, followed by a monotonic bluening which probably lasts beyond the end of our photometric coverage around +40 d.

(five epochs), but only the three epochs close to maximum light have been calibrated and published (Krisciunas et al. 2004)

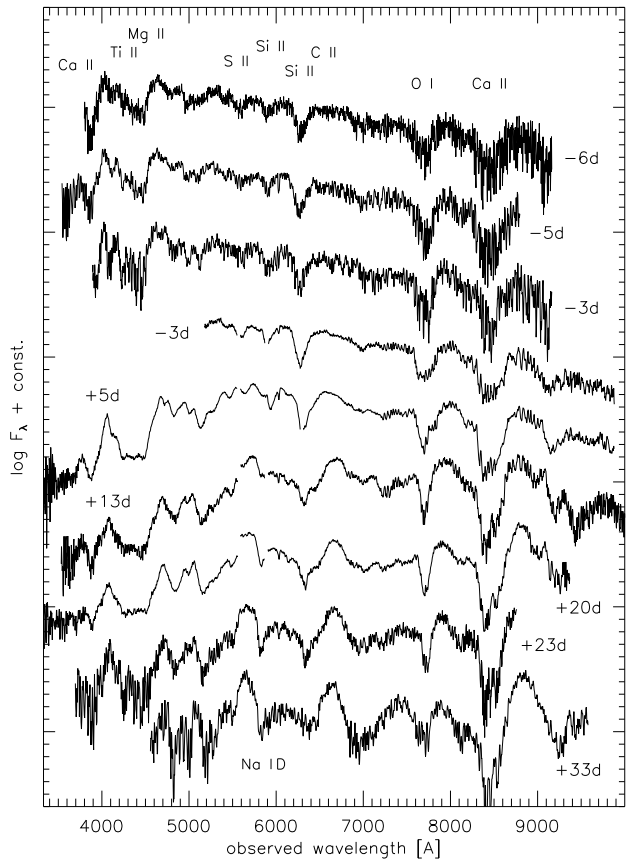


**Figure 8.** Time sequence of SN 2005bl spectra in the observer frame. The phases reported next to each spectrum are with respect to  $B$ -band maximum. The  $-3$  d (blue part) and  $+33$  d spectra have been smoothed using kernel sizes of  $600 \text{ km s}^{-1}$ . Gaps in the TNG spectra indicate the positions of the strongest night-sky residuals, which have been cut in order to avoid confusion with true SN or host-galaxy features (see Section 2.2 and Table 6).

Such a high degree of similarity between different colour indices is not encountered in normal-luminosity SNe Ia (cf. Section 7.1).

## 5 SPECTROSCOPIC EVOLUTION

### 5.1 Spectra of SN 2005bl

The spectra of SN 2005bl presented in Fig. 8 cover the interval from 6 d before to 33 d after  $B$ -band maximum light, i.e., the photospheric phase and the early transition stages towards the nebular phase. During this entire period, the SN follows the evolution of other SNe Ia, in particular of the 91bg-like subclass. The pre-maximum spectra have a blue continuum, with characteristic P-Cygni lines of Si II, S II, Ca II and Mg II superimposed. With respect to normal-luminosity SNe Ia, additional strong Ti II absorptions are visible, and the Si II  $\lambda 5972$  and O I  $\lambda 7774$  absorptions are more pronounced. Shortly after maximum light the blue flux decreases significantly, and also the S II and Si II  $\lambda 5972$  lines fade rapidly, and are no longer detectable two weeks after maximum. Si II  $\lambda 6355$  is, like most other photospheric lines, somewhat more persistent, and can still be discerned beyond

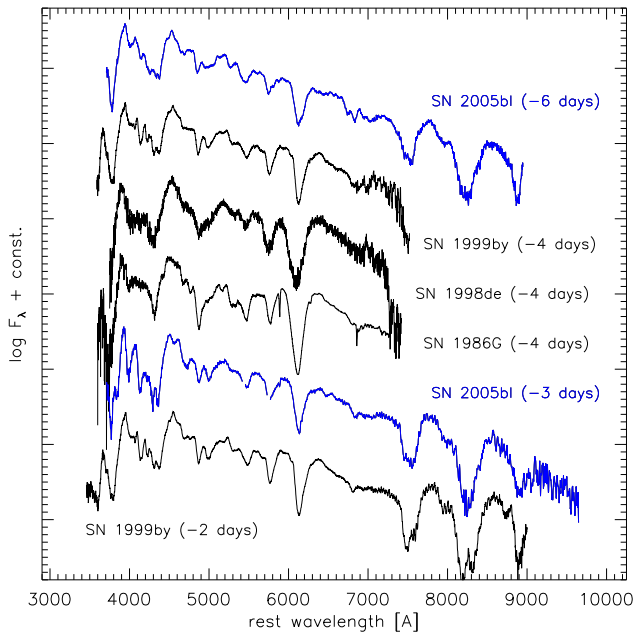


**Figure 9.** Comparison of pre-maximum spectra of underluminous SNe Ia. The spectra were reddening-corrected according to the  $B - V$  colour excesses reported in Section 7. The  $-6$  d spectrum and the blue part of the combined  $-3$  d spectrum of SN 2005bl were boxcar smoothed using kernel sizes of  $2300$  and  $3400 \text{ km s}^{-1}$ , respectively.

$+20$  d. Na I D shows a trend opposite to that of Si and S, first being just visible as a shoulder in the blue wing of the Si II  $\lambda 5972$  line on day  $+5$ , but evolving to a distinct absorption feature by day  $+20$ . In the same period, Fe II emission lines start to dominate the spectrum.

## 5.2 Spectroscopic comparison with other underluminous SNe Ia

In Figs. 9 to 11 the spectra of SN 2005bl are compared with those of other underluminous SNe Ia at epochs of about  $-5$  d,  $+4$  d and  $+30$  d, respectively. For illustration, a comparison with the spectra of the intermediate decliner SN Ia 2004eo ( $\Delta m_{15}(B)_{\text{true}} = 1.46$ , Pastorello et al. 2007b) is made in Fig. 12. The figures show that 91bg-like SNe form a relatively homogeneous spectroscopic subclass, distinct from SNe Ia with normal luminosity and even from those with  $\Delta m_{15}(B)_{\text{true}}$  close to 1.5.

Already at  $-5$  d (Fig. 9) the underluminous SNe Ia show evident Ti features between  $4000$  and  $4400 \text{ \AA}$ , which are absent in SN 2004eo (Fig. 12) where this region is dominated by Si and Mg lines. At the same time Fig. 12 suggests that at  $-6$  d the continuum temperatures are not too different, indicating that the strength of the Ti features in 91bg-like SNe may not be a pure temperature effect but require a truly larger Ti abundance (see also Section 6.2). In SN 1986G (Phillips et al. 1987) the Ti lines are less pronounced than in SNe 1998de (Matheson et al. 2007), 1999by (Garnavich et al. 2004) and 2005bl, emphasising its transitional character between “normal” and strictly 91bg-like SNe Ia. Also, the absolute depth of the Si II  $\lambda 6355$  line in SN 1986G resembles more that of SN 2004eo than those

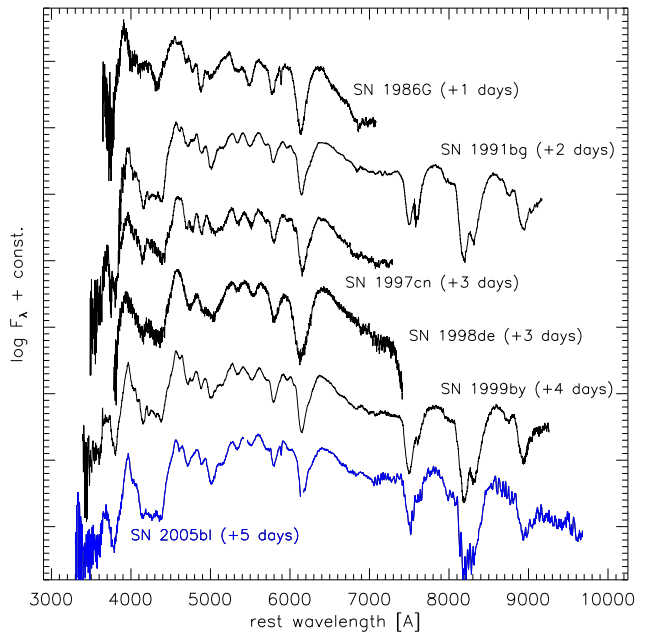


**Figure 10.** The same as Fig. 9, but some days after maximum light in  $B$ .

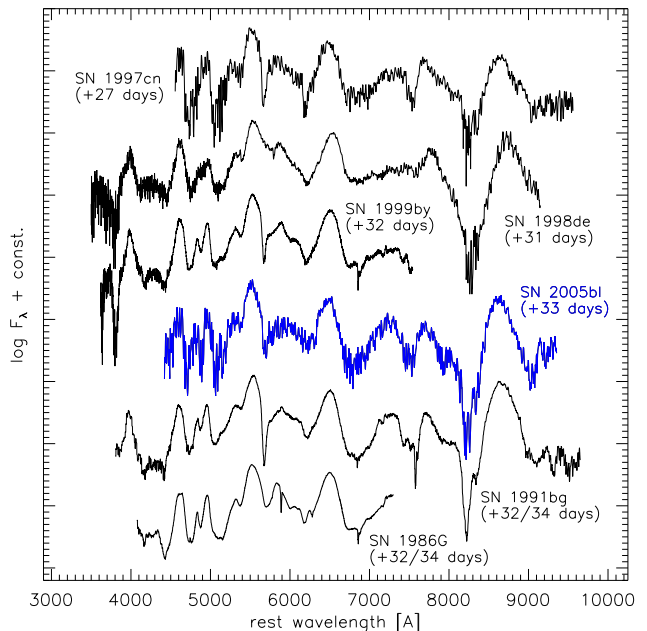


**Figure 11.** The same as Fig. 9, but 4–5 weeks after maximum light in  $B$ . The spectra of SNe 1997cn and 2005bl were smoothed using kernel sizes of  $600 \text{ km s}^{-1}$ .

of SNe 1999by and 2005bl. The Si II lines and most other features of SN 1998de at day  $-5$  are broader and at bluer wavelength than in the other SNe of the sample. The spectra of SNe 2005bl and 1999by are essentially identical, the only exception being the flux depletion in SN 2005bl redwards of the Si II  $\lambda 6355$  line at  $-6$  and  $-5$  d, which we attribute to C II  $\lambda 6580$  (see also Section 7.4). O I  $\lambda 7774$  is particularly pronounced in all underluminous SNe Ia for which the spectral region is covered.

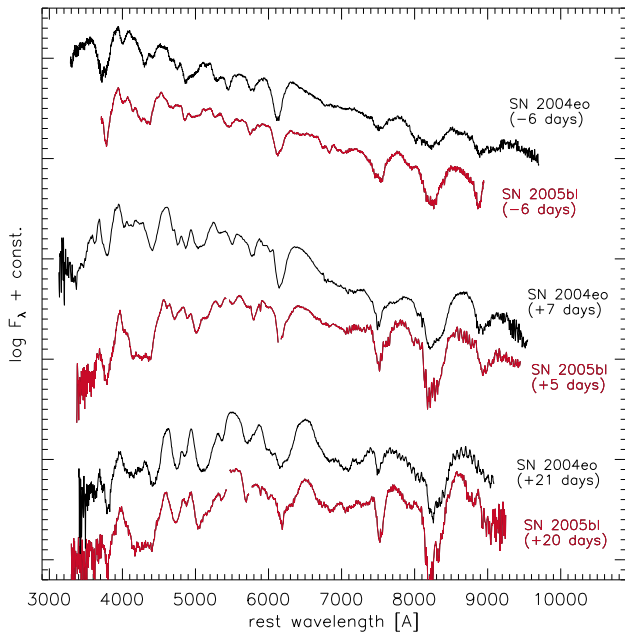


**Figure 12.** Spectroscopic comparison of SN 2005bl and the intermediate decliner SN 2004eo (Pastorello et al. 2007b) at three different epochs. The spectra of SN 2004eo have been dereddened for  $E(B - V) = 0.109$  mag; the  $-6$  d spectrum of SN 2005bl was smoothed using a kernel of  $2300 \text{ km s}^{-1}$ .

By a few days after maximum light (Fig. 10) the spectra have evolved significantly with the continuum being much redder now, but the degree of homogeneity is still remarkably high. The Ti troughs in the blue are now fully developed, showing the characteristic flat bottom that distinguishes 91bg-like from other SNe Ia (Fig. 12). The W-shaped Si II lines around  $5500 \text{ \AA}$  are comparatively weak. Again SN 1986G takes an intermediate position, with the characteristic properties of the underluminous class being less pronounced than in the other objects shown in Fig. 10.

The spectra taken 4–5 weeks past maximum (Fig. 11) reveal that at those phases the transition to the nebular phase has already started. Emission lines of Fe-group elements are visible, but the pseudo-continuum has not yet vanished. Ca II, O I and the Ti trough are still prominent in absorption, while Si II lines cannot be identified any longer. A characteristic feature of many 91bg-like SNe Ia at those epochs is the remarkably narrow Na I D absorption near  $5700 \text{ \AA}$ . Especially in SNe 1991bg (Filippenko et al. 1992b; Leibundgut et al. 1993; Turatto et al. 1996), 1997cn (Turatto et al. 1998) and 1999b by this line is very deep and distinct, while it is less pronounced in SNe 2005bl and, in particular, 1986G and 1998de (Modjaz et al. 2001), where also the narrow core is absent. As already noted by Modjaz et al. (2001), SN 1998de deviates significantly from other 91bg-like SNe between  $6800$  and  $7700 \text{ \AA}$ , exhibiting a relatively smooth continuum without strong O I  $\lambda 7774$  feature.

Unfortunately, no late-time spectra of SN 2005bl were obtained, so that it cannot be verified whether the distinct, broad nebular emission feature near  $7300 \text{ \AA}$ , which characterises SN 1991bg and distinguishes it from ordinary SNe Ia

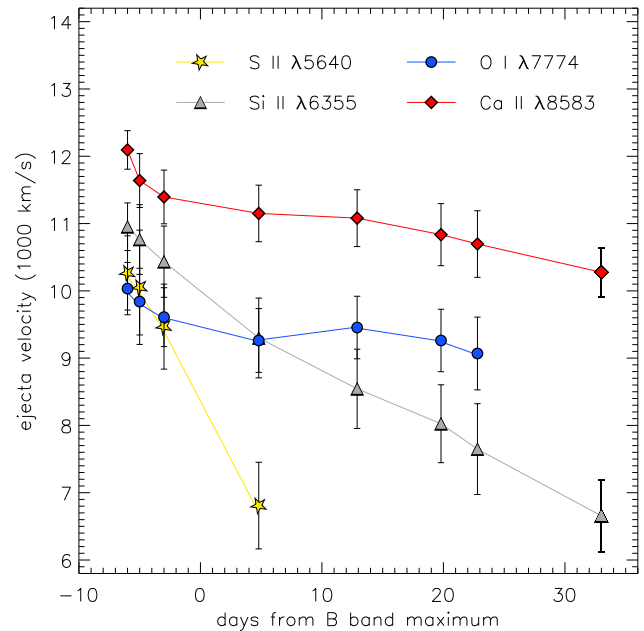


**Figure 13.** Expansion velocities of Si II  $\lambda 5640$ , Si II  $\lambda 6355$ , O I  $\lambda 7774$  and the Ca II NIR-triplet as measured from the minima of the P-Cygni line profiles in SN 2005bl.

at late epochs (Filippenko et al. 1992b; Turatto et al. 1996; Mazzali et al. 1997), is also present in SN 2005bl.

### 5.3 Ejecta velocities

Although ejecta velocities inferred from the blueshift of the absorption minima of P-Cygni lines suffer from a number of uncertainties (such as the typically strong line blending in SN Ia spectra), they do provide important information about the kinetic energy of the ejecta, and can be used as an observationally accessible parameter for comparison studies between different SNe. Furthermore, the range of velocities encompassed by different elements provides insight into the chemical stratification of the ejecta, and hence into nucleosynthesis conditions. This fact has recently been made use of in the Zorro diagnostics (Mazzali et al. 2007). In SNe Ia, especially the Si II  $\lambda 6355$  has proved to be a suitable velocity indicator, since the line is usually well pronounced, fairly unblended and well visible over a relatively long period.

The Si line velocity in SN 2005bl (Fig. 13) evolves from  $\sim 11000 \text{ km s}^{-1}$  at  $-6$  d to  $\sim 6600 \text{ km s}^{-1}$  at  $+33$  d. At maximum light, it is about  $10000 \text{ km s}^{-1}$ , which is low for a SN Ia. The velocity evolution of Si II  $\lambda 5640$  resembles that of Si II, but the temporal decrease is steeper, and the absolute values are systematically lower by  $500$ – $2500 \text{ km s}^{-1}$ , meaning that the line predominantly forms in deeper layers of the ejecta (note that the line is visible only until  $+5$  d). The Ca II IR triplet, on the other hand, has higher velocities than Si II, and the difference increases from about  $1000 \text{ km s}^{-1}$  at  $-6$  d to  $3500 \text{ km s}^{-1}$  at  $+33$  d. This relatively shallow decrease in velocity means that Ca II lines mainly form well above the photosphere. Finally, O I  $\lambda 7774$  also exhibits a fairly constant velocity of  $9000$ – $10000 \text{ km s}^{-1}$  during the entire period of our observations, but this result is not very robust as the feature may be substantially blended with Mg II  $\lambda 7890$ .

## 6 SPECTRAL MODELLING

A 1D Monte-Carlo spectrum synthesis code (Mazzali 2000) was used to simulate the radiation-transport processes in the expanding ejecta of SN 2005bl. Basic assumptions include spherical symmetry, a Chandrasekhar-mass explosion, and an underlying density profile adopted from the W7 explosion model of Nomoto, Thielemann & Yokoi (1984). No attempt was made to obtain better results altering these ingredients. Synthetic fits to four early-time spectra of SN 2005bl were obtained and are presented here, after a short introduction to the concept of the code and the underlying model.

### 6.1 Concept of the radiative transfer code

Only a brief outline is given here; for detailed descriptions of the code see Abbott & Lucy (1985), Mazzali & Lucy (1993), Lucy (1999) and Mazzali (2000), where the basic developments are documented.

The radiative transfer is performed above the photosphere, which is located at an adjustable radius  $r_{\text{ph}}$ . Energy deposition from radioactivity is assumed to occur below the photosphere, from which a blackbody continuum is thought to be emitted. In the “atmosphere” above, radiative equilibrium is supposed to hold. Photons interact with lines and scatter on free electrons, but no continuum formation is assumed (Schuster-Schwarzschild approximation). The underlying W7 density profile is scaled to match the epoch of each spectrum, assuming homologous expansion, i.e.  $r = vt$  for each particle.<sup>10</sup> Element abundances are assumed to be homogeneous inside the envelope. They can be freely adjusted in order to match a given observed spectrum.

In our Monte Carlo calculation, radiation packets are followed from their emission at the photosphere through their interaction history, until they either escape or are re-absorbed at the photosphere. The code takes into account scattering processes (on atoms / ions and electrons) as well as photon branching (absorption in an atomic line and subsequent reemission in another). Line optical depths are calculated in the Sobolev approximation, applicable for fast-expanding atmospheres.

Ionisation and excitation conditions are calculated from the radiation-field statistics. This is done using approximate NLTE formulae (see references above), which in principle employ LTE radiative rates, but additionally take into account the dilution of the radiation field. Collision processes are neglected. A radiation temperature  $T_{\text{R}}$ , determining radiative rates, is calculated in each zone of the envelope. As in Mazzali & Lucy (1993) it is chosen such that the mean frequency of the radiation field inside the zone matches that of a blackbody at  $T_{\text{R}}$ . The matter state and the radiation field are iterated until sufficient convergence is achieved. Within this process, the temperature of the inner-boundary blackbody spectrum is adjusted in order to match the bolometric SN luminosity.

Finally, the emitted spectrum is recalculated solving the formal integral, employing source functions obtained from

<sup>10</sup> This is almost exact for our purposes, as the expansion is homologous already  $\sim 10$ s after explosion onset (see e.g. Röpke 2005).

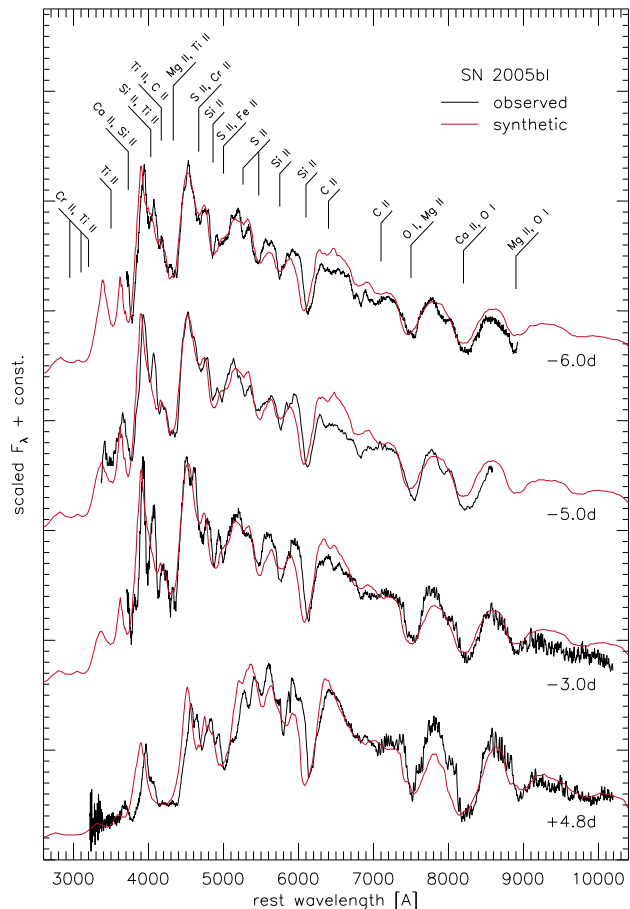


**Figure 14.** Synthetic fits to the SN 2005bl spectra at days  $-6.0$ ,  $-5.0$ ,  $-3.0$  and  $+4.8$ . The observed spectra were smoothed with kernel sizes of  $2300 \text{ km s}^{-1}$  ( $-6.0 \text{ d}$ ) and  $3400 \text{ km s}^{-1}$  ( $-5.0 \text{ d}$  and  $-3.0 \text{ d}$ -blue part) for presentation. The values of relevant fit-parameters are summarised in Table 7. Atop the  $-6 \text{ d}$  spectrum an identification of the most important lines is given.

the packet statistics. This yields smooth spectra at relatively low packet numbers.

### 6.2 Physical parameters and the chemical composition of the models

The basic parameters and composition inferred from the best-fitting synthetic spectra are reported in Table 7. In Fig. 14 these models are compared to the observed spectra, and line identifications for the  $-6 \text{ d}$  spectrum are shown. A rise time to the  $B$ -band maximum of  $17.0 \text{ d}$  is assumed, slightly less than the fiducial value of  $\sim 19.5 \text{ d}$  for normal-luminosity SNe Ia (Riess et al. 1999; Conley et al. 2006). This choice is discussed in Section 7.2.

While the overall shape of the continua is nicely matched and most features are well reproduced, the main shortcomings of the models are a flux excess in the emission component of  $\text{Si II } \lambda 6355$  at early times, and, more worrisome, a mismatch in the position of some lines. Additionally, many synthetic features are too broad and strongly blended, as they were in models for SN 1991bg (Mazzali et al. 1997). No substantial improvement is ob-

**Table 7.** Physical parameters of SN 2005bl inferred from synthetic spectra, assuming a rise time of 17 d in  $B$ . The mass fractions of selected elements are also recorded, and solar photospheric abundances (Asplund, Grevesse & Sauval 2005) are shown for comparison.

	−6.0 d	−5.0 d	−3.0 d	+4.8 d	solar
time from explosion	11.0 d	12.0 d	14.0 d	21.8 d	
bolometric luminosity [ergs <sup>−1</sup> ]	$1.24 \times 10^{42}$	$1.56 \times 10^{42}$	$2.06 \times 10^{42}$	$2.56 \times 10^{42}$	
photospheric velocity [km s <sup>−1</sup> ]	7500	7350	7100	6000	
photospheric blackbody temperature [K]	10 620	10 790	10 670	9230	
X(C)	0.045	0.030	0.010	0.000	$2.16 \times 10^{-3}$
X(O)	0.905	0.878	0.847	0.788	$5.36 \times 10^{-3}$
X(Mg)	0.015	0.040	0.060	0.080	$6.04 \times 10^{-4}$
X(Si)	0.025	0.037	0.060	0.090	$6.66 \times 10^{-4}$
X(S)	0.006	0.009	0.013	0.020	$3.24 \times 10^{-4}$
X(Ti)	$3.7 \times 10^{-4}$	$7.3 \times 10^{-4}$	$1.4 \times 10^{-3}$	$4.5 \times 10^{-3}$	$2.79 \times 10^{-6}$
X(Cr)	$3.7 \times 10^{-4}$	$7.3 \times 10^{-4}$	$1.4 \times 10^{-3}$	$4.5 \times 10^{-3}$	$1.66 \times 10^{-5}$
X(stable Fe)	$1.0 \times 10^{-4}$	$1.2 \times 10^{-4}$	$4.0 \times 10^{-4}$	$1.4 \times 10^{-3}$	$1.15 \times 10^{-3}$
X( <sup>56</sup> Ni + decay products)	–	–	$2.0 \times 10^{-4}$	$2.5 \times 10^{-3}$	

tained reducing the photospheric velocity  $v_{\text{ph}}$ , which indicates that the W7 density profile may not be perfectly suitable for 91bg-like SNe, and that a steeper density gradient may be required. With  $v_{\text{ph}} = 7500 \text{ km s}^{-1}$  6 d prior to maximum light, the inferred photospheric velocity is significantly lower than in normal SNe Ia ( $\sim 10\,000$  to  $11\,000 \text{ km s}^{-1}$  at comparable epochs). By day +5,  $v_{\text{ph}}$  further decreases by about  $1500 \text{ km s}^{-1}$ . Singly and doubly ionised species dominate the ejecta. Especially the singly ionised species leave strong imprints on the spectra, as can be seen from the line identification in Fig. 14. In all spectra modelled here the heavy-element content is comparatively low, but Table 7 shows that it increases with time, indicating composition stratification in the ejecta.<sup>11</sup> At the higher velocities the ejecta are almost entirely made up of unburned material, whereas NSE elements are essentially absent. In particular, no Ni and Co, and only very little Fe are included in the −6 and −5 d models. After maximum light, IMEs and Fe-group elements become more abundant, but still less so than in normal-luminosity SNe Ia (cf., e.g., Stehle et al. 2005). Interestingly, Ti and Cr, whose abundances can be well constrained from the depth of the characteristic trough between 4000 and 4400 Å, appear to be more abundant than Ni, Co and Fe, yet another indication for explosion conditions which disfavour burning to NSE.

## 7 DISCUSSION

In a number of works (e.g. Filippenko et al. 1992b; Leibundgut et al. 1993; Ruiz-Lapuente et al. 1993; Turatto et al. 1996; Mazzali et al. 1997; Turatto et al. 1998; Modjaz et al. 2001; Garnavich et al. 2004) 91bg-like SNe Ia have been studied and found to be different from normally luminous SNe Ia in several respects. Besides their lower luminosity, they have rapidly declining light curves which do not show the characteristic secondary maximum in

<sup>11</sup> For this reason it would be necessary to work with the stratified version of the code (Stehle et al. 2005) if accurate abundances were required. This reaches beyond the scope of this paper. Therefore, the composition reported in Table 7 reflects the overall trend, but the absolute numbers should be taken with caution.

the near-IR, cooler spectra with significant Ti II absorption troughs, low ejecta velocities and large values of the  $\mathcal{R}(\text{Si})$  parameter (Nugent et al. 1995). Nevertheless, the light-curve width and peak luminosity of underluminous SNe Ia seem to obey a correlation (Garnavich et al. 2004), but not the same one as more ordinary SNe Ia. Also, 91bg-like SNe seem to fit smoothly into the Zorro plot (Mazzali et al. 2007), where they represent the extremely <sup>56</sup>Ni-poor, IME-rich end of the SN Ia distribution (but see Section 7.4 for a revised picture). With the increasing number of well-observed objects of this class, it is interesting to revisit some of the aspects mentioned above and to investigate in more detail the degree of homogeneity, or rather diversity, that these SNe exhibit. In Table 8 elementary information on our comparison sample of rapidly-declining SNe Ia is collected; selection criteria were a reasonably dense light-curve coverage starting at least around maximum light, and  $\Delta m_{15}(B)_{\text{true}} > 1.5$ .

### 7.1 Photometric behaviour of underluminous SNe Ia

Here we focus on the photometric properties of underluminous SNe Ia, compare their light-curve shapes and colour indices, determine their peak absolute magnitudes, and investigate their decline-rate vs. luminosity relationship.

#### Light- and colour-curve morphology

Fig. 15 compares the  $B$ ,  $V$  and  $I$  light curves of all the objects in Table 8, rescaled to coincide at maximum light.

The SNe with  $\Delta m_{15}(B)_{\text{true}} \sim 1.9$  (red symbols in Fig. 15), including SN 2005bl, show a single-peaked broad  $I$ -band light curve, whose maximum is delayed by a few days with respect to that in  $B$ . In contrast, the SNe with  $\Delta m_{15}(B)_{\text{true}} \sim 1.5$  to 1.75 (green symbols) clearly

<sup>12</sup> For SN 1986G the Cepheid measurement does not refer to the actual host galaxy Centaurus A, but to NGC 5253, which is a member of the same group (Ferrarese et al. 2000). It was adopted here for the lack of more reliable distance estimates.

**Table 8.** Comparison sample of SNe Ia with  $\Delta m_{15}(B)_{\text{true}} > 1.5$ , ordered by increasing  $\Delta m_{15}(B)_{\text{true}}$ .

SN	$\Delta m_{15}(B)_{\text{true}}$	$M_{B,\text{max}}$	$M_{V,\text{max}}$	$\mathcal{R}(\text{Si})_{\text{max}}$	$i^a$	$E(B-V)^b$	$\mu^c$	morph. <sup>d</sup>	references
1990af	1.57(0.05)	-18.96(0.25)	-18.98(0.19)			0.07(0.06)	36.59(0.05)	SB0	H96a, H96b, P99
2000dk	1.57(0.09)	-18.84(0.18)	-18.83(0.17)			0.07(0.03)	34.18(0.13)	E	J06, VSNET
1999gh	1.69(0.05)	-18.60(0.30)	-18.73(0.28)			0.06(0.03)	32.82(0.25)	E2	J06, VSNET
1992bo	1.69(0.05)	-18.61(0.17)	-18.59(0.15)			0.03(0.03)	34.34(0.12)	SB0 <sub>pec</sub>	H96a, H96b, P99
1993H	1.70(0.10)	-18.57(0.25)	-18.73(0.20)	0.50(0.05)	73(8)	0.12(0.06)	35.07(0.09)	SBab(rs)	H96a, H96b, P99
1986G	1.81(0.07)	-17.76(0.32)	-18.03(0.26)	0.60(0.04)	68(4)	0.78(0.07)	27.61(0.11)	S0 <sub>pec</sub>	H87, P87, P99, F00, B05
1998bp	1.83(0.06)	-17.73(0.25)	-18.08(0.24)			0.08(0.03)	33.13(0.22)	E	G04, J06
1997cn	1.88(0.10)	-17.17(0.20)	-17.79(0.19)	0.68(0.07)	75(9)	0.03(0.03)	34.25(0.13)	E	T98, B05, J06
1999by	1.90(0.05)	-17.17(0.26)	-17.65(0.25)	0.69(0.05)	97(4)	0.02(0.03)	30.75(0.23)	Sb	T00, H01, V01, G04, VSNET
2005bl	1.93(0.10)	-17.24(0.34)	-17.85(0.27)	0.63(0.06)	99(9)	0.20(0.08)	35.10(0.09)	E	this work
1991bg	1.94(0.10)	-16.85(0.34)	-17.56(0.29)	0.66(0.05)	106(5)	0.08(0.06)	31.28(0.20)	E1	F92, L93, T96, P99, F00, T01
1999da	1.95(0.10)	-16.98(0.22)	-17.65(0.20)			0.06(0.03)	33.58(0.17)	SA0	K01
1998de	1.95(0.09)	-16.74(0.19)	-17.43(0.17)	0.69(0.04)	146(3)	0.06(0.03)	34.06(0.14)	S0	M01, J06

<sup>a</sup> Post-maximum decrease of the Si II  $\lambda 6355$  velocity in  $\text{km s}^{-1} \text{d}^{-1}$ , see Benetti et al. (2005) and Section 7.3. <sup>b</sup> Total (Galactic + host galaxy) colour excess. <sup>c</sup> Distance modulus from Cepheids (SNe 1986G and 1999by)<sup>12</sup>, SBF and PNLf (SN 1991bg) or the host galaxy recession velocity with respect to the CMB rest frame (NED) assuming  $H_0 = 72 \text{ km s}^{-1} \text{Mpc}^{-1}$  (other SNe). For the latter, an uncertainty of  $300 \text{ km s}^{-1}$  has been adopted to account for the galaxies' peculiar motions. <sup>d</sup> Host-galaxy morphology (from LEDA). <sup>e</sup> Spectropolarimetry (Hough et al. 1987) indicates  $R_V = 2.4 \pm 0.13$  for the dust in Centaurus A, the host of SN 1986G. We adopted this value and propagated the assigned error to the uncertainty in the absolute magnitudes.

H96a = Hamuy et al. (1996a); H96b = Hamuy et al. (1996b); P99 = Phillips et al. (1999); J06 = Jha et al. (2006); H87 = Hough et al. (1987); P87 = Phillips et al. (1987); F00 = Ferrarese et al. (2000); B05 = Benetti et al. (2005); G04 = Garnavich et al. (2004); T98 = Turatto et al. (1998); T00 = Toth & Szabo (2000); H01 = Howell et al. (2001); V01 = Vinkó et al. (2001); F92 = Filippenko et al. (1992b); L93 = Leibundgut et al. (1993); T96 = Turatto et al. (1996); T01 = Tonry et al. (2001); K01 = Krisciunas et al. (2001); M01 = Modjaz et al. (2001); VSNET = Variable Star Network

have double-peaked  $I$ -band light curves, and, as in normal-luminosity SNe Ia, the first  $I$ -band peak precedes that of the  $B$  band (e.g. Hamuy et al. 1996c; Leibundgut 2000). These observations are in agreement with the results of Kasen (2006), who computed synthetic light curves with the SEDONA code, varying the mass of  $^{56}\text{Ni}$ . His prediction is an ever smaller temporal offset of the first and secondary  $I$ -band maxima with decreasing SN luminosity, and the merging to a single broad peak for the most underluminous objects. The  $B$ -band light curves of the two groups (red and green symbols in Fig. 15) also exhibit noticeable differences in shape, probably influenced by the evolution of the Ti trough. 91bg-like SNe settle to the radioactive tail earlier, only  $\sim 15$  d after maximum light. Consequently, the drop in magnitude from the peak to the tail is smaller for these, although their initial decline is steeper. Thus, the  $B$  light curves of 91bg-like and “normal” SNe Ia cannot be transformed into each other by employing a simple stretch factor.

The only objects in the sample with  $1.75 \leq \Delta m_{15}(B)_{\text{true}} < 1.85$  are SNe 1986G and 1998bp (yellow symbols). The light-curve morphology of these SNe seems to provide a link between the formerly defined groups. While the  $I$  band is still single-peaked with maybe a hint of a double peak, the luminosity drop from maximum to the radioactive tail in the  $B$  band resembles that of SNe with  $\Delta m_{15}(B)_{\text{true}} < 1.75$ . The existence of objects with such intermediate properties might support the idea of a common progenitor and explosion scenario for *all* SNe Ia. However, SN statistics tell us that objects with  $\Delta m_{15}(B)_{\text{true}} \approx 1.8$  are intrinsically rare.

Fig. 16 shows the reddening-corrected  $B-V$  and  $V-I$  colour curves of the same SNe as above. The differences in  $B-V$  after +30 d are marginal, and all SNe obey the Lira (1995) relation within the uncertainties (note, however, that for the more strongly-reddened SNe 1986G and 2005bl the Lira relation was directly or indirectly used to infer the true extinction along the line of sight, making this a circular argument). On the contrary, the  $B-V$  colour evolution around maximum light shows remarkable differences, the 91bg-like SNe Ia having a much redder colour at maximum (0.4 to 0.7 mag, compared to  $\sim 0.0$  mag for SNe Ia with  $\Delta m_{15}(B)_{\text{true}} < 1.75$ ). Also, the peak  $B-V$  colour is reached earlier in underluminous SNe, and is redder by  $\sim 0.3$  mag.

In  $V-I$  the differences among the objects of Table 8 are even more pronounced. The  $V-I$  colour index of SNe Ia with  $1.50 < \Delta m_{15}(B)_{\text{true}} < 1.75$  decreases from about 10 d before to 5–10 d after  $B$ -band maximum just like in all intermediate or slow decliners, then increases steeply, levelling off at  $\sim 20$  d and again decreasing slowly thereafter. 91bg-like SNe, in contrast, do not show the initial bluening, but become redder from the very first available observations onwards. This behaviour continues until  $\sim 15$  d past maximum, when the curves flatten and subsequently a soft bluening sets in. Evidently, the origin of the different  $V-I$  evolution lies in the different delay of the main maximum and the presence or absence of the secondary maximum in the  $I$  band.

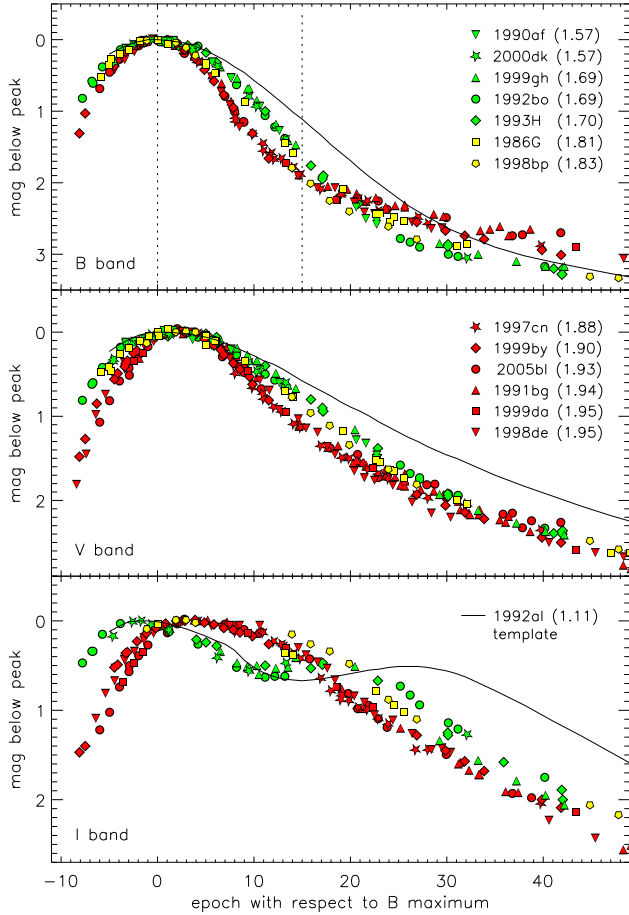


**Figure 15.** *BVI* light curves of the rapidly-declining SNe Ia of Table 8, normalised to their peak magnitudes. The  $\Delta m_{15}(B)_{\text{true}}$  of each SN is given in parentheses. Different symbol colours represent different decline rates (green:  $1.50 < \Delta m_{15}(B)_{\text{true}} < 1.75$ ; yellow:  $1.75 \leq \Delta m_{15}(B)_{\text{true}} < 1.85$ ; red:  $\Delta m_{15}(B)_{\text{true}} \geq 1.85$ ). Light-curve templates of SN 1992al ( $\Delta m_{15}(B)_{\text{true}} = 1.11$ , Hamuy et al. 1996c) are shown for comparison.

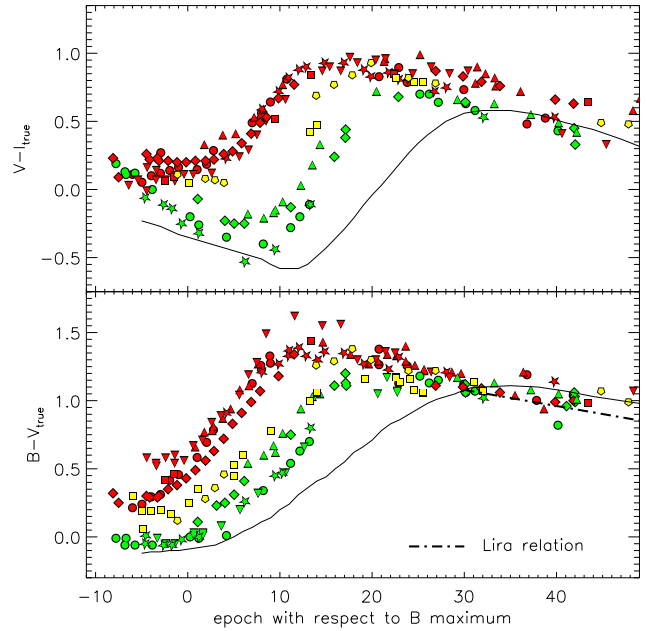
### Absolute magnitudes & Phillips relation

Table 8 shows that the peak absolute magnitudes of the SNe with  $\Delta m_{15}(B)_{\text{true}} > 1.5$  span a wide range, from  $-16.74$  to  $-18.96$  in the *B* band. As Hamuy et al. (1996a), Phillips et al. (1999) and Garnavich et al. (2004) pointed out, also for these SNe the peak magnitudes correlate with  $\Delta m_{15}(B)_{\text{true}}$ , but the dependence is steeper than for more slowly declining SNe Ia. Based only on SNe with  $\Delta m_{15}(B)_{\text{true}} \geq 1.69$ , our best linear fits (Fig. 17) are given by

$$M_{B,\text{peak}} = -18.54 + 5 \log(H_0/72) + 6.83 (\Delta m_{15}(B)_{\text{true}} - 1.7)$$

$$M_{V,\text{peak}} = -18.61 + 5 \log(H_0/72) + 4.33 (\Delta m_{15}(B)_{\text{true}} - 1.7).$$

The slopes of  $6.83 \pm 0.32$  and  $4.33 \pm 0.31$  for the *B* and *V* bands are in excellent agreement with the results of Garnavich et al. (2004), and much steeper than what Hamuy et al. (1996a) find for SNe with  $\Delta m_{15}(B)_{\text{true}} \leq 1.69$  ( $0.78 \pm 0.17$  and  $0.71 \pm 0.14$  for *B* and *V*, respectively). Also the quadratic relation derived by Phillips et al. (1999) for SNe with  $\Delta m_{15}(B)_{\text{true}} < 1.70$  provides a poor fit to the peak magnitudes of fast decliners.



**Figure 16.** Evolution of the *B* – *V* (top panel) and *V* – *I* (bottom panel) colour indices of the rapidly-declining SN Ia sample of Table 8 plus SN 1992al. The symbols and colour coding are the same as in Fig. 15. The dash-dotted line in the lower panel represents the Lira (1995) relation, i.e. the uniform *B* – *V* colour that all SNe Ia are supposed to exhibit between day +30 and +90.

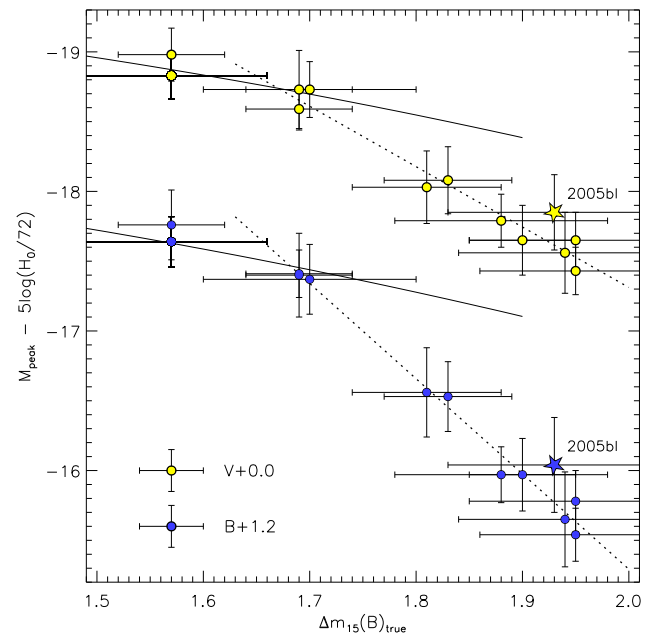


**Figure 17.** Peak absolute *B*- and *V*-band magnitudes of the SN sample of Table 8. The dotted lines are the best linear fits to the data with  $\Delta m_{15}(B)_{\text{true}} \geq 1.69$ , characterised by slopes of  $6.83 \pm 0.32$  and  $4.33 \pm 0.31$  for *B* and *V*, respectively. The solid lines show the quadratic relation obtained by Phillips et al. (1999) for SNe Ia with  $\Delta m_{15}(B)_{\text{true}} < 1.70$ .

## 7.2 The rise time of underluminous SNe Ia

Rise times of SNe Ia are important to constrain possible explosion models. In our synthetic spectra the rise time  $t_r$  determines the actual (scaled) density profile at a given epoch (cf. Section 6.1), and hence the matter density of the line-forming region. Here we report our attempts to estimate the rise time of 91bg-like SNe, in particular of SN 2005bl.

### Photometric rise-time determination

Efforts have been made to measure SN-Ia rise times directly from a fit to their early-time light curves (Riess et al. 1999; Conley et al. 2006; Strovink 2007). Depending on measurement details, these studies yield rise times of 17 to 20 d for fiducial  $\Delta m_{15}(B)_{\text{true}} = 1.1$  SNe Ia. Furthermore, there seems to be a negative correlation between  $t_r$  and  $\Delta m_{15}(B)_{\text{true}}$ , faster decliners having shorter rise times. However, all these studies are based on samples of “normal” SNe Ia with  $\Delta m_{15}(B)_{\text{true}} \leq 1.5$ , and it may be doubted whether the inferred trends can be extrapolated to 91bg-like SNe with  $\Delta m_{15}(B)_{\text{true}} \approx 1.9$ .

What makes these direct measurements so demanding is the need for high-quality early-time photometry, preferentially before day  $-10$  (Riess et al. 1999), which to date is not available for any 91bg-like SN, including 2005bl. In order to constrain the rise times of this class of objects, it may be useful to consider the two 91bg-like SNe Ia with the earliest photometric data, SNe 1998de and 1999by. Both have a filtered light-curve coverage starting about one week before  $B$ -band maximum, complemented by earlier unfiltered measurements and some deep detection limits shortly before. For SN 1998de the earliest detection showing just “a hint of the supernova” was on unfiltered CCD frames taken 12.3 d before  $B$ -band maximum (preceded by a non-detection down to a limiting magnitude of 19.0 five days earlier, Modjaz et al. 1998), thus providing at least a lower limit for the rise time. For SN 1999by, the earliest detection on unfiltered CCD frames dates back to day  $-11.4$ , showing the SN at only  $5 \pm 1\%$  of the peak  $R$ -luminosity (Arbour et al. 1999). Further detection limits constrain the SN luminosity to be less than  $\sim 1.6\%$  of the peak value at  $-12.4$  d, and less than  $\sim 0.3\%$  at  $-15.1$  d. Applying the method described by Riess et al. (1999) to these data, but using unfiltered and  $R$ -band points between  $-11.4$  and  $-4.0$  d for the fit (Fig. 18), a rise time to  $B$ -band maximum of  $13.9_{-1.1}^{+1.2}$  would be inferred for SN 1999by, the errors being the  $3\text{-}\sigma$  confidence levels of the fit combined with the uncertainty in determining the epoch of  $B$ -band maximum (Garnavich et al. 2004).

In this approach we disregarded a possible (and theoretically not unexpected) deviation from the early  $L \propto t^2$ -behaviour which is the basis of the Riess et al. analysis. If the synthesised  $^{56}\text{Ni}$  is confined to the inner ejecta, which – at least for 91bg-like objects – is supported by the lack of Ni in the  $-6$  and  $-5$  d spectra of SN 2005bl (cf. Section 6.2), it should require some time for the photons to reach the photosphere and be released. This could result in an initial post-explosion phase with only very little brightening of the SN, before the observed steep rise of the light curve sets in. For this reason, the inferred value of 13.9 d might be considered a *lower limit* to the actual rise time of SN 1999by. Given the similarity in terms of light-curve shape, this re-

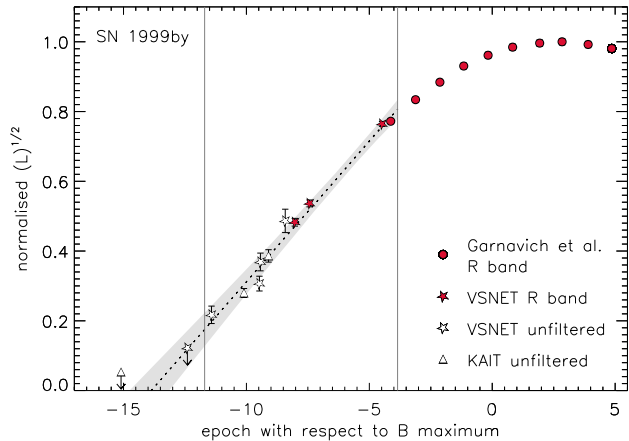


**Figure 18.** R-band/unfiltered early-time light curve of SN 1999by, plotted as  $L^{1/2}$  vs.  $t - t_{B_{\text{max}}}$ , and linear fit (dotted line) to the data up to day  $-4$  (between the two thin vertical lines). Assuming  $L \propto t^2$ , the instance of explosion would be given by the intersection of the fit with  $L^{1/2} = 0$  at  $-13.9$  d. The grey-shaded region marks the  $3\text{-}\sigma$  confidence bands of the linear fit. Caveats are discussed in the text.

sult should provide a good indication also for the rise time of SN 2005bl.

### The rise time addressed by spectral modelling

The rise time constitutes an important input parameter for our spectrum synthesis calculations. Since the colour of an observed spectrum has to be reproduced in a corresponding model, the photospheric temperature, which can be crudely approximated through the Stefan-Boltzmann-law  $L \propto v_{\text{ph}}^2 t^2 T^4$ , is confined to a limited range. Assuming a shorter rise time, the photospheric velocity thus usually has to be increased in order to keep the photospheric temperature constant. The line velocities in the synthetic spectrum then also tend to be larger.

Given the difficulties in observational rise-time determination, we created eight models with different rise times (12.5–25.0 d) for the earliest available spectrum of SN 2005bl ( $-6$  d), where a change in  $t_r$  has the largest relative effect. Excluding models largely deviating from the observed spectrum yielded a range of acceptable rise times. For the models with  $t_r < 14.0$  d, we had to use photospheric velocities of  $v_{\text{ph}} > 10\,200 \text{ km s}^{-1}$ , which are incompatible with observed and measured (Fig. 13) O I and Si II expansion velocities. Choosing rise times of 14.0–15.5 d, most weaker lines were fitted nicely, while in stronger lines such as Si II  $\lambda 6355$  or Ca II H&K there was still a lack of absorption at low velocity. While weaker lines mostly form near the photosphere, strong lines have considerable strength also in layers well above. Thus, their centroid typically shows a larger blueshift, and their emission, centred at the rest wavelength, is more pronounced. In order to decrease the flux in their red wings,  $v_{\text{ph}}$  had to be reduced to 5000–6000  $\text{km s}^{-1}$ , corresponding to rise times of 22–20 d. The weaker features, however, then appeared at velocities too low in the synthetic spectrum.

The difficulty to match all line-velocities simultaneously points to some substantial shortcoming in our treatment of the SN ejecta. Stratifying the ejecta composition

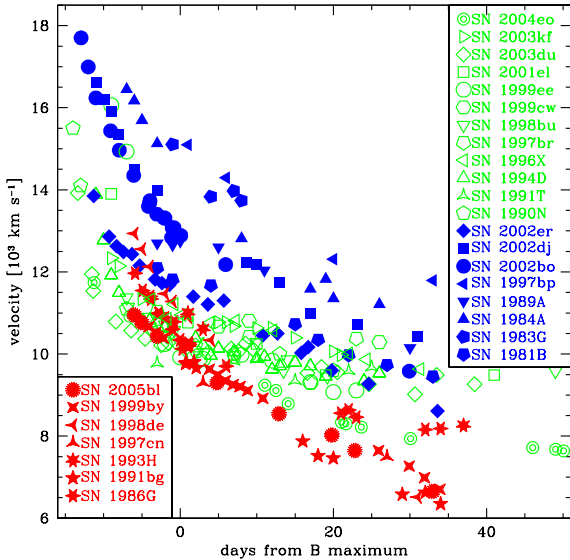


**Figure 19.** Velocity measured from the minimum of the Si II  $\lambda 6355$  line as a function of time. Open green symbols represent low-velocity-gradient (LVG) SNe, filled blue symbols high-velocity-gradient (HVG) SNe, and red starred symbols correspond to the FAIN'T SNe, as defined by Benetti et al. (2005). The values for HVG and LVG SNe are taken from Benetti et al. and Pastorello et al. (2007b), while the data set for the FAIN'T class has been extended and in parts remeasured.

(Stehle et al. 2005) assuming only little Si and Ca at high velocity might cure some of the problems, as it could potentially remove the blue parts of the respective strong absorption lines and reduce their re-emission. Yet, we retained our uniform-abundance approach, because no observational data earlier than  $-6$  d are available to constrain the additional parameters of a stratified-abundance model. Alternative explanations for the inconsistencies include a possible inadequacy of the W7 density structure, a deviation of the total ejected mass from  $M_{\text{Ch}}$ , or 3D effects.

Nonetheless, based on our model sequence, we confidently exclude rise times shorter than 14 and longer than 22 d. For all spectral models discussed below we assumed a rise time of 17.0 d. This value is fully compatible with the lower limits observationally derived above. At the same time, it is slightly shorter than what is favoured for  $\Delta m_{15}(B)_{\text{true}} = 1.1$ -SNe, in agreement with the trend found for SNe Ia with  $\Delta m_{15}(B)_{\text{true}} \leq 1.5$  (e.g. Riess et al. 1999; Kasen & Woosley 2007).

### 7.3 Spectroscopic parameters

A spectroscopic comparison of SN 2005bl with other underluminous SNe Ia was performed in Section 5.2, in particular in Figs. 9–11. Here, we concentrate on parameters such as  $\mathcal{R}(\text{Si})$  (Nugent et al. 1995) and  $\dot{v}$  (the average daily rate of velocity decrease of Si II  $\lambda 6355$  between  $B$ -band maximum and either the time the Si II feature disappears or the last available spectrum, whichever is earlier; Benetti et al. 2005). With respect to Benetti et al. (2005), these param-

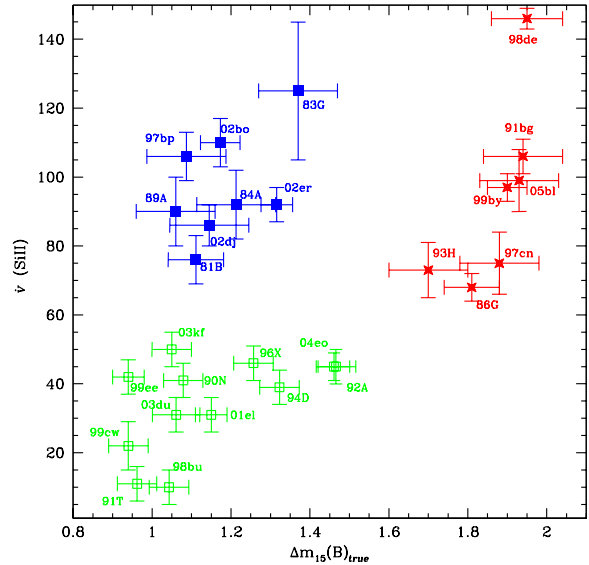


**Figure 20.** Si II  $\lambda 6355$  post-maximum velocity gradient  $\dot{v}$  (Benetti et al. 2005) versus  $\Delta m_{15}(B)_{\text{true}}$ . Filled blue squares are HVG SNe, open green squares LVG SNe, and filled red stars FAIN'T SNe.

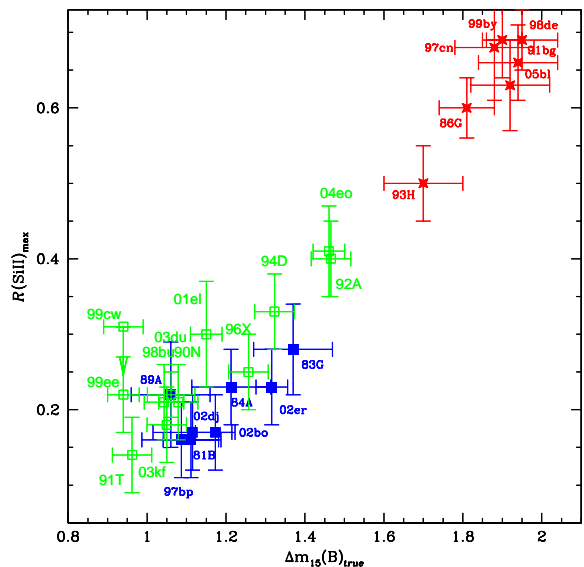


**Figure 21.** Si line-depth ratio  $\mathcal{R}(\text{Si})_{\text{max}}$  (Nugent et al. 1995) as a function of SN decline rate  $\Delta m_{15}(B)_{\text{true}}$ . The strong correlation between these two parameters is evident. Symbols as in Fig. 20.

eters have been remeasured for some FAIN'T SNe using additional data, and SNe 1998de (Matheson et al. 2007) and 2005bl have been added.

Fig. 19 shows the velocity evolution of the Si II  $\lambda 6355$  line of SN 2005bl and a large set of comparison objects. Once more, SN 2005bl is extremely similar to SNe 1991bg, 1997cn and 1999by. Before maximum light, the Si velocities

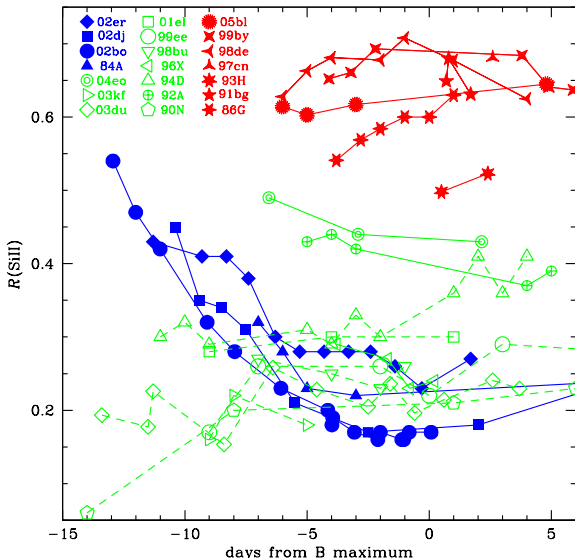


**Figure 22.** Time-evolution of the Nugent et al. (1995) ratio  $\mathcal{R}(\text{Si})$  before and near maximum light. The same symbols as in Fig. 19 have been used. Interpolating lines between adjacent points have been drawn to guide the eye.

of these SNe are comparable to those of the slower members of Benetti et al.’s LVG group, but the velocity decrease is much faster. Hence, after maximum light, they have clearly the lowest expansion velocities. SN 1998de, photometrically nearly a twin of SN 2005bl, has noticeably higher expansion velocities at early phases. Whether this is caused by a high-velocity component (Mazzali et al. 2005), by differences in the density structure, or by a higher kinetic energy is difficult to decide without detailed modelling. High-velocity features could provide a natural explanation for the observed differences without the need to change the explosion energetics. On the other hand the Si II  $\lambda 6355$  line of SN 1998de looks symmetric, and the velocities are higher than in other 91bg-like SNe not only at the earliest phases, but also near maximum light, when in most other SNe the high-velocity features have disappeared (Mazzali et al. 2005; Garavini et al. 2007). Finally, the transitional SNe 1993H and 1986G have higher velocities than SN 2005bl and the other 91bg-like SNe (except SN 1998de), more similar to the LVG group. Their comparatively shallow post-maximum velocity decrease  $\dot{v}$  (Benetti et al. 2005) also shows their proximity to LVG SNe.

In the  $\dot{v}$  vs.  $\Delta m_{15}(B)_{\text{true}}$  plane, FAINT SNe seem to form a separate cluster (Fig. 20). However, this impression may be caused by the lack of SNe with  $\Delta m_{15}(B)_{\text{true}}$  between 1.5 and 1.7 in the Benetti et al. sample. Whether or not this gap is real is not easy to decide given the poor statistics for rapidly-declining SNe Ia. With respect to  $\dot{v}$  alone, FAINT SNe are very heterogeneous, with values ranging from those typical of LVG SNe to the highest values ever recorded in a SN Ia (for SN 1998de). The mean  $\dot{v}$  of  $95 \pm 27$  (statistical)  $\text{km s}^{-1} \text{d}^{-1}$  is similar to that reported by Benetti et al. for HVG SNe ( $97 \pm 16 \text{ km s}^{-1} \text{d}^{-1}$ ). Within the FAINT group there may be a tendency for higher  $\dot{v}$  with

larger  $\Delta m_{15}(B)_{\text{true}}$ , but there are too few objects and their range in  $\Delta m_{15}(B)_{\text{true}}$  is too small to postulate a correlation.

Concerning  $\mathcal{R}(\text{Si})_{\text{max}}$ , the value of  $\mathcal{R}(\text{Si})$  at  $B$ -band maximum, we confirm the observed trend of larger values for faster decliners (Fig. 21). The origin of this behaviour was the subject of a number of studies, as an explanation is not straightforward. Hachinger, Mazzali & Benetti (2006) have shown that the change in  $\mathcal{R}(\text{Si})_{\text{max}}$  with  $\Delta m_{15}(B)_{\text{true}}$  is almost solely caused by a variation in the strength of the Si II  $\lambda 5972$  line, which is somewhat counter-intuitive as the excitation of this line should be favoured by higher temperatures. Garnavich et al. (2004) suggested that in underluminous SNe Ia the feature at  $\sim 5800 \text{ \AA}$  might be dominated by Ti lines. However, from the synthetic spectra shown in Section 6.2 we cannot confirm this option. Instead, Hachinger (2007, and in prep.) demonstrate that the observed tendency is a combined ionisation and excitation effect, natural rather than unexpected.

The pre-maximum time-evolution of  $\mathcal{R}(\text{Si})$ , which was also used by Benetti et al. (2005) to distinguish between the LVG and HVG groups, cannot be studied equally well for the FAINT SNe because of the lack of sufficiently early data (more than 5d before maximum). In fact, only before day  $-5$  do LVG and HVG SNe show significant differences in their behaviour,  $\mathcal{R}(\text{Si})$  decreasing with time for HVG SNe, and being constant or increasing slightly for LVG SNe. Near maximum light, the evolution seems to be fairly flat for all SNe Ia, including the FAINT SNe which merely exhibit larger absolute values of  $\mathcal{R}(\text{Si})$  (see Fig. 22). However, especially the Si II  $\lambda 5972$  line may suffer from variable contributions of other elements, notably Na I D at later phases when the spectra become cooler. This limits the conclusive power of all studies related to the evolution of  $\mathcal{R}(\text{Si})$  after maximum light, as already at day  $+5$  Na I D is visible as a shoulder in the blue wing of the Si II  $\lambda 5972$  feature (cf. Section 5.1).

#### 7.4 Element abundances from synthetic spectra

Spectrum synthesis calculations offer an insight into the chemical composition of the ejecta, making it possible to trace the nuclear reactions that took place during explosive burning. However, because of the limitations and possible shortcomings of the models mentioned in Section 6 (i.e., no abundance stratification, use of a Chandrasekhar-mass progenitor and of the W7 density distribution), the exact numbers in Table 7 should be taken with caution. Therefore, we confine ourselves to analysing clear trends, which should be robust with respect to refined models.

#### Unburned material, carbon detection

As for all rapidly-declining SNe Ia the spectrum of SN 2005bl is characterised by strong O I  $\lambda 7774$ . The strength of this line is largely a temperature effect, as the comparatively low temperatures encountered in 91bg-like SNe Ia result in a fair fraction of neutral oxygen besides the singly ionised state which normally dominates the ejecta. Nevertheless, it also signals the presence of a significant amount of un-

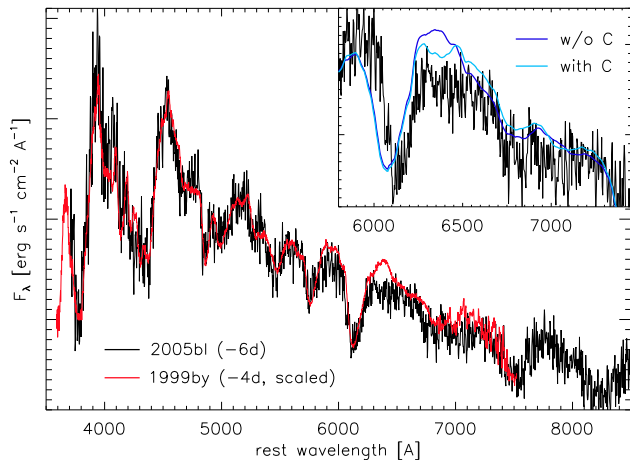


**Figure 23.** Identification of carbon in the spectra of SN 2005bl. A comparison of the  $-6$  d spectrum of SN 2005bl and the  $-4$  d spectrum of SN 1999by shows a flux deficit at  $6400 \text{ \AA}$  in SN 2005bl, likely caused by C II  $\lambda 6580$ . The insert shows synthetic spectra for day  $-6$ , one with the composition reported in Table 7 including 4.5% of C, the other without any C.

burned material in the SN ejecta.<sup>13</sup> This is fully consistent with the often-anticipated low burning efficiency of these objects (from light curves and nebular spectra one can infer that the amount of synthesised  $^{56}\text{Ni}$  is  $\sim 0.1 M_{\odot}$ , which is at most a quarter of that in normal-luminosity SNe Ia, Stritzinger et al. 2006). Direct information on the oxygen abundance is difficult to derive from synthetic spectra, since O I  $\lambda 7774$  is the only strong feature of this element at optical wavelengths, and is heavily saturated in all our models. Hence, moderate changes in the oxygen content have no impact on the strength of this feature. Additionally, our abundance estimate should be considered an upper limit, as, guided by nuclear reaction network calculations, we ascribe the entire mass without observable signatures to oxygen.

Applying this strategy, we find oxygen mass fractions ranging from  $> 90\%$  at day  $-6$  to  $\sim 80\%$  at day  $+5$ . With a W7 density profile and photospheric velocities of  $7500$  and  $6000 \text{ km s}^{-1}$ , about 50 and 60% of the ejecta mass are located above the photospheres at days  $-6$  and  $+5$ , respectively. Hence, if a Chandrasekhar-mass explosion with W7 density profile provides an acceptable model for 91bg-like SNe Ia, at least the outer 50% of the ejecta of SN 2005bl and other members of this group are entirely dominated by unburned material. These numbers are significantly different from the results obtained by modelling normal SNe Ia (cf., e.g., Stehle et al. 2005). They are also in disagreement with the picture sketched in the Zorro plot (Mazzali et al. 2007), i.e. that all LVG and FAINT SNe Ia have about the same amount of unburned material, and that the observed spectrophotometric sequence among SNe Ia has its origin only in a variable ratio of  $^{56}\text{Ni}$  to IMEs.

Another indication of the low burning efficiency in SN 2005bl is the likely detection of unprocessed carbon in its

early spectra. Although the S/N of the  $-6$  and  $-5$  d spectra is low, a clear flux deficit redwards of the Si II  $\lambda 6355$  absorption can be discerned compared to coeval spectra of SN 1999by (Fig. 23).

Synthetic spectra enable us to investigate the effect of including different chemical species on this region. There are only few lines which could potentially contribute to the observed absorption.<sup>14</sup> Including hydrogen did not improve the model, since the resulting H $\alpha$  absorption was at too short a wavelength, and H $\alpha$  emission deteriorated the fit around  $6500 \text{ \AA}$ . A clearly better match to the observed spectrum was obtained introducing carbon, as C II lines not only cropped the flux peak at  $6400 \text{ \AA}$  through C II  $\lambda 6580$  (Fig. 23, insert), but also improved the fit in other regions, most notably around  $7000 \text{ \AA}$  (through C II  $\lambda 7234$ ). Therefore, we consider the presence of a few percent of carbon in the ejecta at days  $-6$  and  $-5$  very likely.

The temperature and density conditions for carbon burning are more relaxed than those for oxygen burning, so that carbon is burned much more completely to heavier elements than oxygen. In fact, only in some – usually very early ( $\sim -10$  d) – optical spectra of SNe Ia have clear signatures of carbon ever been found (most prominently in SN 2006gz, Hicken et al. 2007; cf. also Branch et al. 2007 for an overview). None of these SNe was 91bg-like, although the lower burning efficiency in these objects might favour the presence of unprocessed carbon. The lack of spectra taken earlier than 5 d before maximum light may have so far prevented the detection of carbon. In SN 2005bl, however, we are confident that signatures of carbon are present less than one week before maximum. This constitutes one of the few detections of C II in SN Ia spectra at such a relatively late epoch; previous cases include SNe 1996X and 2006D (Thomas et al. 2007).

### Abundance of Fe-group elements

The Fe-group abundance of SN 2005bl of  $\sim 0.01\%$  at day  $-6$  and  $\sim 0.4\%$  at day  $+5$  is about two orders of magnitude lower than in normal-luminosity SNe Ia at comparable epochs (see, e.g., Stehle et al. 2005; Kotak et al. 2005; Elias-Rosa et al. 2006; Altavilla et al. 2007). At a first glance this looks perfectly consistent with the low luminosity and hence the low production of  $^{56}\text{Ni}$  and other NSE-elements in a 91bg-like SN Ia.

However, closer examination reveals that the Fe content of the pre-maximum models is significantly sub-solar. At  $-6$  d the best-fitting model contains no Ni or Co, and only 0.010 % of stable Fe. Acceptable results were obtained with Fe abundances up to 0.025 %, but also without any Fe (see Fig. 24). Solar Fe abundances (the Fe mass fraction of the Sun’s photosphere is about 0.115 %, Asplund et al. 2005) can safely be ruled out, as with this amount of Fe the

<sup>13</sup> In this section we refer to C and O as unburned, although – depending on the initial C-to-O ratio of the white dwarf – a significant fraction of the O may have been produced during the explosion by incomplete C burning.

<sup>14</sup> Conversely, because of the relative lack of strong lines, the region around  $6400 \text{ \AA}$  proved to be a preferential window for flux redistributed from shorter wavelengths to escape. All elements which create opacity in the blue and UV part of the spectrum (Fe-group elements, Ti, Cr, other metals) rather led to an increase of the  $6400 \text{ \AA}$  flux excess in the model. This in turn yielded constraints on the metal abundance.

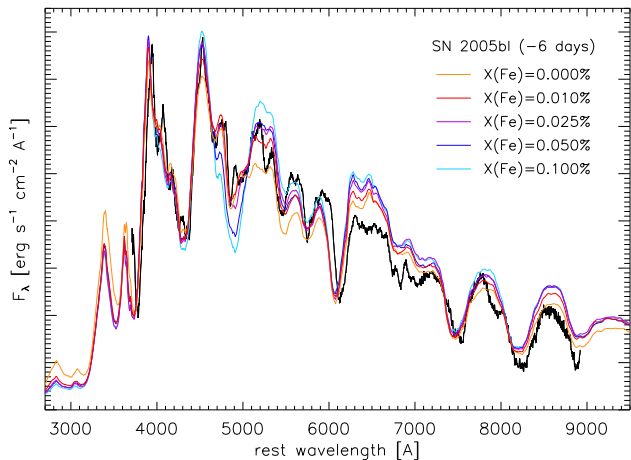


**Figure 24.** Sequence of synthetic spectra, varying the mass fraction of Fe between 0 to 0.1% (the latter roughly represents solar Fe abundance). The observed but smoothed  $-6$  d spectrum is shown in black. The parameters of the best-fitting spectrum (with  $X(\text{Fe})=0.01\%$ ) are summarised in Table 7. The other spectra have been obtained by changing only the amount of stable Fe at the expense of O, the most abundant element, without attempting to optimise the fit by adapting other parameters. Hence, better fits might be feasible also for the models with  $X(\text{Fe}) \neq 0.01\%$ .

quality of the fit deteriorates a lot around  $5000 \text{ \AA}$ . Now, the Fe content deduced not only accounts for  $^{54}\text{Fe}$  synthesised during the explosive burning (the  $^{56}\text{Ni}$  decay chain has too long decay times to give a relevant contribution at these epochs), but also for Fe already present in the progenitor star before the explosion. Hence, a sub-solar Fe content of the precursor star might be inferred. On the other hand, SN 2005bl exploded in an elliptical galaxy, a presumably not metal-poor environment. If the chemical composition of the precursor did not deviate significantly from the average material in NGC 4070, it rather should have had a fairly high Fe abundance, and nuclear burning should have further enriched the ejecta with Fe-group elements, although this may be confined to the inner shells.

There may be two ways to explain the small amount of Fe required to fit the early-time spectra of SN 2005bl. One is to assume that Fe was not distributed homogeneously in the progenitor star, but concentrated towards the centre. A certain degree of gravitational settling of heavier elements can indeed be expected. Estimating whether or not this effect is sufficient to yield Fe abundances in accordance to those inferred from the synthetic spectra would require a model of gravitational diffusion inside the white dwarf, and accurate constraints on the mass accretion rate from the companion and the composition of the accreted material. Note, however, that assuming  $v_{\text{ph}} = 7500 \text{ km s}^{-1}$  and a W7 density profile the photosphere at day  $-6$  is not located in the outermost layers, but half the way down the ejecta in mass coordinates.

Alternatively, the progenitor of SN 2005bl might have had a metallicity truly lower than the average metallicity of an elliptical galaxy. This could be explained if the progenitor was rather old ( $\sim 10$  Gyr), formed before the ISM in NGC 4070 was metal-enriched through recurrent cycles of stellar birth, mass loss and death. If this scenario held true, it would provide one of the first direct constraints on the

lifetime of an individual SN Ia progenitor. Given the spectroscopic similarity of SN 2005bl to SNe 1991bg, 1997cn, 1998de and 1999by, and given that most of the latter SNe also exploded in early-type, supposedly metal-rich galaxies (see Table 8), this could point towards a very long-lived progenitor population for *all* underluminous, 91bg-like SNe Ia.

A speculation could be that 91bg-like SNe Ia descend from white-dwarf mergers (DD scenario). White-dwarf binary systems should meet the requirement of long lifetimes because of the low efficiency of angular-momentum loss through gravitational-wave emission. In fact, in a study of the delay-time distribution of SNe Ia, Greggio (2005) identified initially wide white-dwarf pairs as the only progenitor model whose delay-time distribution does not drop dramatically beyond  $\sim 8$  Gyr. Models of Kobayashi et al. (1998) lend further support to the DD scenario, as they predict that no SNe Ia should occur in SD systems for  $[\text{Fe}/\text{H}] \leq -1$ , a limit which may be exceeded by SN 2005bl. Finally, from spectropolarimetric observations of SN 1999by Howell et al. (2001) inferred a degree of asphericity much higher than in ordinary SNe Ia. On this basis they identified rapidly rotating white dwarfs and merging white-dwarf binaries as the most promising progenitor candidates for 91bg-like SNe Ia. A different progenitor system with respect to ordinary SNe Ia (for which the SD scenario consisting of a white dwarf and a non-degenerate companion is favoured), and in particular the possibility that the mass is different from  $M_{\text{Ch}}$ , could account for observed differences in the photometric and spectroscopic properties of 91bg-like SNe.

## 8 CONCLUSIONS

We have presented and analysed optical photometric and spectroscopic data of the underluminous Type Ia SN 2005bl from one week before to two months after maximum light in  $B$ . In this entire interval the evolution of SN 2005bl is substantially different from that of slow or intermediate decliners, but very similar to that of the prototypical fast decliners SNe 1991bg and 1999by. At peak, SN 2005bl appears slightly more luminous than the latter, but the difference is marginal and within the error bars, which for SN 2005bl are dominated by uncertainties in the amount of host-galaxy extinction. With respect to quantities like the  $\Delta m_{15}(B)_{\text{true}}$  of 1.93, the ejecta velocities inferred from the minimum of the  $\text{Si II } \lambda 6355$  line, and temperature indicators such as  $\mathcal{R}(\text{Si})$  or the time-evolution of various colour indices, SN 2005bl is in fact – within the measurement uncertainties – a clone of SNe 1991bg and 1999by.

We confirm that  $\Delta m_{15}(B)_{\text{true}}$  is a good luminosity indicator also for underluminous SNe Ia, with a steeper dependence of the peak magnitudes on  $\Delta m_{15}(B)_{\text{true}}$  than for slow and intermediate decliners. From linear fits we obtain  $\frac{d(M_{\text{peak}})}{d(\Delta m_{15}(B)_{\text{true}})} = 6.83 \pm 0.32$  and  $4.33 \pm 0.31$  for the  $B$  and  $V$  band, respectively, considering objects with  $\Delta m_{15}(B)_{\text{true}} \geq 1.69$ .

We conducted an analysis analogous to that of Benetti et al. (2005), focussing on the behaviour of the FAINT subclass and trying to identify trends within this group. In addition to the SNe in Benetti et al. we not only added the measurements of SN 2005bl, but also included SN 1998de (Modjaz et al. 2001; Matheson et al. 2007) and

updated some numbers on the basis of better data availability. We find a correlation between  $\Delta m_{15}(B)_{\text{true}}$  and  $\mathcal{R}(\text{Si})_{\text{max}}$ , nicely extending the observed linear trend among HVG and LVG SNe to larger decline rates. Because of the lack of early data, the time-evolution of  $\mathcal{R}(\text{Si})$  at phases where differences between the LVG and HVG groups become evident cannot be investigated. The Si II line velocities of FAINT SNe are mostly similar to those of LVG SNe near maximum light, but significantly lower a few weeks later. There is a large dispersion in post-maximum velocity gradients  $\dot{v}$  within the FAINT class, with numbers comparable to those of HVG SNe, but exceeding their range in both directions.

Synthetic spectra for SN 2005bl at four epochs before and soon after maximum light have been computed using a 1D Monte Carlo code. Despite uncertainties and shortcomings such as the poorly-constrained rise time, the possible inadequacy of the W7 density profile for 91bg-like SNe Ia, and the fact that computations were performed without chemical stratification, a number of interesting results were obtained. The presence of carbon in the  $-6$  and  $-5$  d spectra, indicated by a visual comparison with SN 1999by at similar epoch, was confirmed, and an overall low burning efficiency was established. NSE elements, but also IMEs, are significantly less abundant than in ordinary SNe Ia; instead, most of the ejecta above  $6000 \text{ km s}^{-1}$  are made of oxygen, and are hence either unburned or the result of highly incomplete carbon burning. Furthermore, in the  $-6$  and  $-5$  d spectra only traces of Fe are found, one order of magnitude less than expected for unprocessed material with solar composition. Possible implications of this low metallicity on the nature of the progenitor were discussed in Section 7.4.

It is presently very difficult to decide whether 91bg-like SNe Ia form a separate group, distinct from ordinary SNe Ia and possibly descending from different progenitors or explosion mechanisms, or whether they are just the extreme end of a continuous distribution of objects, with their characteristic appearance owing to lower temperatures in conjunction with a different chemical composition, both caused by the overall low burning efficiency. To tackle this problem will require a new statistical analysis similar to that of Benetti et al. (2005) once a bigger sample of rapidly-declining SNe Ia will be available, and more detailed spectral modelling of the data sets already published.

## ACKNOWLEDGMENTS

S.T. is grateful to Thomas Matheson for kindly providing access to unpublished spectra of SN 1998de obtained with the 1.5 m Tillinghast Telescope + FAST spectrograph.

This work has been supported by the European Union's Human Potential Programme "The Physics of Type Ia Supernovae," under contract HPRN-CT-2002-00303. M.H. acknowledges support from the Centro de Astrofísica FON-DAP 15010003, Proyecto Fondecyt 1060808, and Núcleo Milenio P06-045-F. G.P. acknowledges support by the Proyecto Fondecyt 3070034.

The paper is based on observations collected at the 2.5 m du Pont and the 1.0 m Swope Telescopes (Las Campanas, Chile), the 2.2 m Telescope of the Centro Astronómico Hispano Alemán (Calar Alto, Spain), the Asiago

1.82 m and the Loiano 1.52 m Telescopes (INAF observatories, Italy), the Italian 3.58 m Telescopio Nazionale Galileo and the 2.0 m Liverpool Telescope (La Palma, Spain), the Wendelstein 0.8 m Telescope (Bavaria, Germany), and the ESO Very Large Telescope (Cerro Paranal, Chile). The Telescopio Nazionale Galileo is operated by the Fundación Galileo Galilei of the INAF (Istituto Nazionale di Astrofisica) at the Spanish Observatorio del Roque de los Muchachos of the Instituto de Astrofísica de Canarias. Our thanks go to the support astronomers at the Telescopio Nazionale Galileo, the Loiano 1.52 m Telescope and the 2.2 m Telescope in Calar Alto for performing the follow-up observations of SN 2005bl.

This research made use of the NASA/IPAC Extragalactic Database (NED) which is operated by the Jet Propulsion Laboratory, California Institute of Technology, under contract with the National Aeronautics and Space Administration, and the Lyon-Meudon Extragalactic Database (LEDA), supplied by the LEDA team at the Centre de Recherche Astronomique de Lyon, Observatoire de Lyon.

## REFERENCES

- Abbott D. C., Lucy L. B., 1985, *ApJ*, 288, 679  
 Altavilla G., et al., 2007, *A&A*, 475, 585  
 Arbour R., Papenkova M., Li W. D., Filippenko A. V., Armstrong M., 1999, *IAUC* 7156, 1  
 Asplund M., Grevesse N., Sauval A. J., 2005, in Barnes T. G., III, Bash F. N., eds, *ASP Conference Series*, Vol. 336. San Francisco: Astron. Society of the Pacific, p. 25  
 Benetti S., et al., 2005, *ApJ*, 623, 1011  
 Bessell M. S., 1990, *PASP*, 102, 1181  
 Branch D., et al., 2007, *PASP*, 119, 709  
 Cardelli J. A., Clayton G. C., Mathis J. S., 1989, *ApJ*, 345, 245  
 Conley A., et al., 2006, *AJ*, 132, 1707  
 Contardo G., Leibundgut B., Vacca W. D., 2000, *A&A*, 359, 876  
 Elias J. H., Matthews K., Neugebauer G., Persson S. E., 1985, *ApJ*, 296, 379  
 Elias-Rosa N., et al., 2006, *MNRAS*, 369, 1880  
 Ferrarese L., et al., 2000, *ApJ*, 529, 745  
 Filippenko A. V., 1997, *ARA&A*, 35, 309  
 Filippenko A. V., Porter A. C., Sargent W. L. W., Schneider D. P., 1986, *AJ*, 92, 1341  
 Filippenko A. V., et al., 1992a, *ApJ*, 384, L15  
 Filippenko A. V., et al., 1992b, *AJ*, 104, 1543  
 Freedman W. L., et al., 2001, *ApJ*, 553, 47  
 Fukugita M., Ichikawa T., Gunn J. E., Doi M., Shimasaku K., Schneider D. P., 1996, *AJ*, 111, 1748  
 Gallagher J. S., Garnavich P. M., Modjaz M., Kirshner R. P., Challis P., 2005a, *IAUC* 8514, 3  
 Gallagher J. S., Garnavich P. M., Berlind P., Challis P., Jha S., Kirshner R. P., 2005b, *ApJ*, 634, 210  
 Garavini G., et al., 2007, *A&A*, 471, 527  
 Garnavich P. M., et al., 2004, *ApJ*, 613, 1120  
 Greggio L., 2005, *A&A*, 441, 1055  
 Hachinger S., 2007, Diploma thesis, Technische Universität München  
 Hachinger S., Mazzali P. A., Benetti S., 2006, *MNRAS*, 370, 299

- Hamuy M., Phillips M. M., Schommer R. A., Suntzeff N. B., Maza J., Avilés R., 1996a, *AJ*, 112, 2391
- Hamuy M., et al., 1996b, *AJ*, 112, 2408
- Hamuy M., Phillips M. M., Suntzeff N. B., Schommer R. A., Maza J., Smith R. C., Lira P., Avilés R., 1996c, *AJ*, 112, 2438
- Hamuy M., Trager S. C., Pinto P. A., Phillips M. M., Schommer R. A., Ivanov V., Suntzeff N. B., 2000, *AJ*, 120, 1479
- Hicken M., Garnavich P. M., Prieto J. L., Blondin S., Depoy D. L., Kirshner R. P., Parrent J., 2007, *ApJ*, 669, L17
- Hillebrandt W., Niemeyer J. C., 2000, *ARA&A*, 38, 191
- Höflich P., Gerardy C. L., Fesen R. A., Sakai S., 2002, *ApJ*, 568, 791
- Horne K., 1986, *PASP*, 98, 609
- Hough J. H., Bailey J. A., Rouse M. F., Whittet D. C. B., 1987, *MNRAS*, 227, 1
- Howell D. A., 2001, *ApJ*, 554, L193
- Howell D. A., Höflich P., Wang L., Wheeler J. C., 2001, *ApJ*, 556, 302
- Jha S., et al., 2006, *AJ*, 131, 527
- Jordi K., Grebel E. K., Ammon K., 2006, *A&A*, 460, 339
- Kasen D., 2006, *ApJ*, 649, 939
- Kasen D., Woosley S. E., 2007, *ApJ*, 656, 661
- Kobayashi C., Tsujimoto T., Nomoto K., Hachisu I., Kato M., 1998, *ApJ*, 503, L155
- Kotak R., et al., 2005, *A&A*, 436, 1021
- Krisciunas K., et al., 2001, *AJ*, 122, 1616
- Krisciunas K., et al., 2004, *AJ*, 128, 3034
- Landolt A. U., 1992, *AJ*, 104, 340
- Leibundgut B., 2000, *A&ARv*, 10, 179
- Leibundgut B., et al., 1993, *AJ*, 105, 301
- Li W., Filippenko A. V., Treffers R. R., Riess A. G., Hu J., Qiu Y., 2001, *ApJ*, 546, 734
- Li W., et al., 2003, *PASP*, 115, 453
- Lira P., 1995, Master thesis, Univ. Chile
- Lucy L. B., 1999, *A&A*, 345, 211
- Massey P., 1997, A User's Guide to CCD Reductions with IRAF, <http://iraf.noao.edu/docs/recommend.html>
- Massey P., Davis L. E., 1992, A User's Guide to Stellar CCD Photometry with IRAF, <http://iraf.noao.edu/docs/recommend.html>
- Massey P., Valdes F., Barnes J., 1992, A User's Guide to Reducing Slit Spectra with IRAF, <http://iraf.noao.edu/docs/recommend.html>
- Matheson T., et al., 2007, *AJ* submitted
- Mazzali P. A., 2000, *A&A*, 363, 705
- Mazzali P. A., Lucy L. B., 1993, *A&A*, 279, 447
- Mazzali P. A., Danziger I. J., Turatto M., 1995, *A&A*, 297, 509
- Mazzali P. A., Chugai N., Turatto M., Lucy L. B., Danziger I. J., Cappellaro E., Della Valle M., Benetti S., 1997, *MNRAS*, 284, 151
- Mazzali P. A., et al., 2005, *ApJ*, 623, 37
- Mazzali P. A., Röpke F. K., Benetti S., Hillebrandt W., 2007, *Sci*, 315, 825
- Modjaz M., Halderson E., Shefler T., King J. Y., Li W. D., Treffers R. R., Filippenko A. V., 1998, *IAUC* 6977, 1
- Modjaz M., Li W., Filippenko A. V., King J. Y., Leonard D. C., Matheson T., Treffers R. R., Riess A. G., 2001, *PASP*, 113, 308
- Morrell N., Folatelli G., Phillips M., Contreras C., Hamuy M., 2005, *IAUC* 8514, 2
- Nomoto K., Thielemann F.-K., Yokoi K., 1984, *ApJ*, 286, 644
- Nomoto K., Filippenko A. V., Shigeyama T., 1990, *A&A*, 240, L1
- Nugent P., Phillips M., Baron E., Branch D., Hauschildt P., 1995, *ApJ*, 455, L147
- Pastorello A., et al., 2007a, *MNRAS*, 376, 1301
- Pastorello A., et al., 2007b, *MNRAS*, 377, 1531
- Patil M. K., Pandey S. K., Sahu D. K., Kembhavi A., 2007, *A&A*, 461, 103
- Pfannes J. M. M., 2006, PhD thesis, Bayerische Julius-Maximilians-Univ., Würzburg, <http://www.astro.uni-wuerzburg.de/~pfannes/>
- Phillips M. M., 1993, *ApJ*, 413, 105
- Phillips M. M., Phillips A. C., Heathcote S. R., Blanco V. M., Geisler D., Hamilton D., Suntzeff N. B., 1987, *PASP*, 99, 592
- Phillips M. M., Wells L. A., Suntzeff N. B., Hamuy M., Leibundgut B., Kirshner R. P., Foltz C. B., 1992, *AJ*, 103, 1632
- Phillips M. M., Lira P., Suntzeff N. B., Schommer R. A., Hamuy M., Maza J., 1999, *AJ*, 118, 1766
- Pignata G., et al., 2004, *MNRAS*, 355, 178
- Porter A. C., Dickinson M., Stanford S. A., Lada E. A., Fuller G. A., Myers P. C., 1992, *AAS*, 181, 7607
- Pskovskii Y. P., 1984, *SvA*, 28, 658
- Puckett T., Langoussis A., 2005, *IAUC* 8515, 3
- Riess A. G., et al., 1999, *AJ*, 118, 2675
- Röpke F. K., 2005, *A&A*, 432, 969
- Ruiz-Lapuente P., Cappellaro E., Turatto M., Gouffes C., Danziger I. J., Della Valle M., Lucy L. B., 1992, *ApJ*, 387, L33
- Ruiz-Lapuente P., et al., 1993, *Nature*, 365, 728
- Shimasaki K., Li W., 2005, *IAUC* 8512, 2
- Schlegel D. J., Finkbeiner D. P., Davis M., 1998, *ApJ*, 500, 525
- Smith J. A., et al., 2002, *AJ*, 123, 2121
- Spergel D. N., et al., 2003, *ApJS*, 148, 175
- Stehle M., Mazzali P. A., Benetti S., Hillebrandt W., 2005, *MNRAS*, 360, 1231
- Stritzinger M., et al., 2002, *AJ*, 124, 2100
- Stritzinger M., Mazzali P. A., Sollermann J., Benetti S., 2006, *A&A*, 460, 793
- Strovink M., 2007, *ApJ* accepted (arXiv:0705.0726)
- Suntzeff N. B., 1996, in McCray R., Wang Z., eds, *AU Colloquium 145: "Supernovae and Supernova Remnants"*. Cambridge: University Press, p. 200
- Thomas R. C., et al., 2007, *ApJ*, 654, L53
- Tonry J. L., Dressler A., Blakeslee J. P., Ajhar E. A., Fletcher A. B., Luppino G. A., Metzger M. R., Moore C. B., 2001, *ApJ*, 546, 681
- Toth I., Szabo R., 2000, *A&A*, 361, 63
- Turatto M., Benetti S., Cappellaro E., Danziger I. J., Della Valle M., Gouffes C., Mazzali P. A., Patat F., 1996, *MNRAS*, 283, 1
- Turatto M., Piemonte A., Benetti S., Cappellaro E., Mazzali P. A., Danziger I. J., Patat F., 1998, *AJ*, 116, 2431
- Turatto M., Benetti S., Cappellaro E., 2003, in Hillebrandt W., Leibundgut B., eds, *Proceedings to the ESO/MPA/MPE Workshop "From Twilight to Highlight:*

The Physics of Supernovae". Springer, Berlin, p. 200  
Vinkó J., Kiss L. L., Csák B., Fűrész G., Szabó R., Thomson J. R., Mochnacki S. W., 2001, AJ, 121, 3127  
Wang X., et al., 2007, ApJ submitted (arXiv:0708.0140)  
Zhao C., Newberg H. J., 2006, arXiv e-print (astro-ph/0612034)

This paper has been typeset from a  $\text{\TeX}$ / $\text{\LaTeX}$  file prepared by the author.